POLITECNICO DI MILANO

Facoltà di ingegneria Industriale
Corso di Laurea in Ingegneria Energetica

Analysis of heat and moisture transfer in building components by conjugate modeling

Relatore interno: Colombo Luigi Pietro Maria

Correlatore: Bianchi Janetti Michele

Tesi di laurea di:
Lorenzo Nespoli
Matr: 783288

Anno Accademico 2012/2013

Contents

Nomenclature

α	convective heat transfer coefficient	[W/m^{2}K]
β	convective mass transfer coefficient	[s/m]
η	small eddies characteristic length	[m]
γ	generic convective flux	[1/m^{2}s]
μ	vapour resistance factor	[–]
ν_w	dynamic viscosity of water	[kg/m^3]
ϕ	material porosity	[–]
ρ_v	vapour density	[kg/m^3]
ρ_w	water density	[kg/m^3]
ρ_g	total gas density	[kg/m^3]
σ	water surface tension	[N/m]
θ_c	contact angle	[rad]
φ	relative humidity	[–]
A_u	unscaled absolute tolerance	[–]
C_m	moisture content	[kg/m^3]
c_p	thermal capacity at constant pressure	[J/kgK]
D_{av}	binary diffusion coefficient for water vapour in air	[m^2/s]
$D_{e\varphi a}$	relative humidity driven heat transfer coefficient in air	[W/m]
$D_{e\varphi p}$	relative humidity driven heat transfer coefficient in porous material	[W/m]
D_{eTa}	temperature driven heat transfer coefficient in air	[W/mK]
D_{eTp}	temperature driven heat transfer coefficient in porous material	[W/mK]
$D_{m\varphi a}$	relative humidity driven mass transfer coefficient in air	[kg/ms]
$D_{m\varphi p}$	relative humidity driven mass transfer coefficient in porous media	[kg/ms]

D_{mTa}	temperature driven mass transfer coefficient in air [kg/msK]	
D_{mTp}	temperature driven mass transfer coefficient in porous media [kg/msK]	
ETC_{rv}	equivalent thermal conductivity relative variation	[–]
Gr	Grashof number	[–]
H	volumetric enthalpy	[kJ/m^3]
h_l	liquid enthalpy	[kJ/kg]
h_v	vapour enthalpy	[kJ/kg]
H_{ev}	enthalpy of evaporization	[kJ/kg]
J	total mass flux	[kg/m^{2}s]
J^a	advective mass flux	[kg/m^{2}s]
J^c	capillary mass flux	[kg/m^{2}s]
J^d	diffusive mass flux	[kg/m^{2}s]
K_l	capillar conductivity	[s]
k_{eff}	effective thermal conductivity	[W/mK]
L	characteristic length	[m]
L_0	big eddies characteristic length	[m]
M	molar mass	[kg/kmol]
M_f	number of fields	[–]
m_v	vapour mass fraction	[kg$_\mathrm{v}$/kg$_\mathrm{g}$]
N	number of degree of freedom	[–]
P	error of convergence	[–]
p	pressure	[Pa]
p_c	capillary pressure	[Pa]
p_s	saturation pressure	[Pa]
p_w	water pressure	[Pa]
q	convective heat flux	[W/m^2]
q^c	conductive heat flux	[W/m^2]

q^e	enthalpy flux	[W/m^2]
R	universal gas constant	[J/molK]
r_c	capillary radius	[m]
R_h	relative normalized error	[–]
R_t	relative tolerance	[–]
R_v	gas constant for water vapour	[J/kgK]
Re	Reynolds number	[–]
Ri	Richardson number	[–]
U	characteristic velocity	[m/s]
V	average velocity	[m/s]
v'	velocity fluctuation	[m/s]
w	phase content	[kg/m$^3_{\text{pm}}$]
w	water content	[kg/m^3]
w_{cs}	water content at capillary saturation	[kg/m^3]
x_w	molar fraction of water in liquid	[mol/mol$_{\text{liquid}}$]
y_w	molar fraction of water in air	[mol/mol$_{\text{air}}$]
$\mathbf{v}$	velocity	[m/s]
ETC	equivalent thermal conductivity	[W/mK]

Subscripts

a	air
fm	fluid media
l	liquid
m	dry porous material
pm	porous material
s	solid matrix
v	vapour

List of Figures

List of Tables

Acknowledgment

This thesis was written at the Leopold-Franzens-Universität Innsbruck as part of the 3encult project for the energy retrofit of historic buildings.

I wish to express special thanks to Ing. Michele Bianchi Janetti for his availability and his endless patience being my assistant thesis supervisor, and to Dr.-Ing Luigi P.M. Colombo for being my supervisor and for his advices. I also wish to thank Dr.-Ing. Fabian Ochs for making this thesis possible, Prof. Raffaella Pavani for helping me in the numerical part of the thesis, and Thijs Defraeye for his availability.

I thank the members of the Energy Efficient Buildings unit, whom I shared the office with, for their advices and for the games they taught me during lunch time.

Finally I would like to thank my family and my friends for their support during the writing of this thesis.

Abstract

This work presents a numerical analysis of heat and moisture transfer in building components in presence of a convective flow. Numerical simulation can supply important information for a correct design and for the choice of proper materials. At present, specific software for hygrothermal simulation in building-physics application, based on the works of Künzel [33] and Grunewald [19], are available [54],[55] . This software enables HAM (Heat, Air, Moisture) modeling in porous media; however CFD (computational fluid dynamic) and 3D modeling are not yet included.

A coupling approach for the equations of transport in the porous and fluid media is used, avoiding previous calculation of convective heat and mass transfer coefficients. The coupled differential equations are solved using finite element procedure for both gas phase and solid. Since CFD may present high complexity and significant computational effort, also a simplified approach, convenient for long-period simulation, is derived. In the first part of the thesis the mathematical model is described. In the second part both the approaches are validated through comparison with experimental data taken from the literature. Following, the plausibility of the results is investigated for various case studies and comparisons with other simulation programs is performed.

Sommario

Lo studio del contenuto di umidità all'interno degli elementi strutturali di un edificio è importante dal punto di vista energetico, sanitario e strutturale. La presenza di umidità all'interno delle pareti di un edificio può compromettere significativamente le sue capacità isolanti, aumentando la conduttività termica equivalente (ETC) delle pareti. Se i valori di umidità relativa sulla superficie di una parete sono superiori all'80% vi è un elevato rischio di formazione di muffe, con potenziali danni sulla salute degli abitanti della casa. Se i valori di umidità relativa sono prossimi all'unità, si può verificare condensa del vapore acqueo all'interno delle pareti. La condensazione interstiziale su tali elementi può portare al degrado dei materiali e a una conseguente diminuzione delle prestazioni e della durabilità dei materiali.

Le simulazioni numeriche sono uno strumento essenziale per il design di un isolamento che possa garantire la massima efficienza energetica, ed evitare la formazione di condensa.

Queste simulazioni sono particolarmente utili negli studi di energy retrofit su edifici storici. Tali edifici sono spesso di grandi dimensioni, e una corretta coibentazione rappresenta un risparmio in termini energetici ed economici. A causa della rilevanza storica e/o artistica delle pareti esterne, è spesso impossibile applicare un isolamento esterno. Applicare un isolamento interno aumenta i rischi di condense interstiziali fra lo strato isolante e la parete interna dell'edificio. L'applicazione corretta di un isolante termico è particolarmente difficile nel caso in cui siano presenti delle travi passanti in metallo o in legno all'interno delle pareti. In questo caso è sempre presente un intercapedine fra travi e parete, che consente il passaggio di aria umida. Poiché le travi agiscono come ponti termici, in questi punti vi sarà una temperatura più bassa rispetto al resto della parete, rendendo possibile la condensa.

I principali software attualmente disponibili in commercio per analisi igrotermiche, consentono di tener conto dell'influenza della convezione tramite un coefficiente globale di scambio termico e di massa. Questo approccio risulta essere poco accurato rispetto a un modello che consideri l'interazione fra aria e parete con un calcolo fluidodinamico (CFD). Gli studi igrotermici che sfruttano calcoli fluidodinamici per risolvere il campo di moto sono comunemente chiamati coniugati o accoppiati. Attraverso questo approccio, è possibile tener conto dello scambio termico e di umidità senza una conoscenza pregressa dei coefficienti di scambio convettivo.

In questa tesi si è sviluppato un modello computazionale che permetta di studiare l'influenza dei fenomeni convettivi che avvengono all'interno delle intercapedini, sulla distribuzione di umidità e temperatura all'interno dei materiali strutturali, utilizzando un modello coniugato.

Nella prima parte del lavoro, vengono esposti gli attuali metodi di modellazione dello scambio termico e di umidità all'interno dei materiali porosi. Successivamente vengono introdotti e descritti i principali meccanismi di trasporto termico e di massa usati nel modello matematico.

Nel capitolo 3 viene discussa la necessità di utilizzare una modellazione Low

Reynolds nel caso in cui si debba considerare un flusso d'aria turbolento.

Nel capitolo 4 viene esposto lo stato dell'arte nella modellazione dello scambio termico e di umidità fra fluidi e mezzi porosi. Successivamente vengono introdotte le equazioni di bilancio di massa e di energia per il mezzo poroso e per l'aria umida, con le relative assunzioni e restrizioni.

Poiché lo scopo della maggior parte delle simulazioni igrotermiche è quello di indagare gli effetti dell'umidità nel lungo periodo, e poiché le condizioni al contorno di queste simulazioni sono tipicamente tempo varianti, utilizzare una simulazione CFD può portare a un elevato tempo di calcolo. Per questo motivo, in questo capitolo si introducono anche le equazioni di un modello semplificato (approccio line source) . Questo approccio utilizza coefficienti di scambio termico e di massa ricavati dalla letteratura o da simulazioni CFD stazionarie, e consente di tener conto della dipendenza temporale dei valori di bulk di temperatura e umidità all'interno dell'intercapedine.

Nella seconda parte della tesi, i risultati del modello coniugato e del modello line source sono comparati con simulazioni svolte da software commerciali e con dati sperimentali ottenuti dalla letteratura. Nei casi testati, entrambi i modelli restituiscono dei risultati in accordo coi dati disponibili.

Nell'ultima parte del capitolo 5, i risultati dei due modelli vengono confrontati fra loro in un caso in cui un intercapedine subisce una curvatura ad angolo retto, per evidenziare la differenza fra approccio coniugato e line source in presenza di distacco di vena fluida.

Nel capitolo 6 si mostra come il modello coniugato possa essere usato in altre simulazioni di interesse ingegneristico in ambito edilizio. In particolare viene considerata l'influenza dell'umidità sul calcolo dell'ETC di un mattone forato, in presenza di convezione naturale interna.

Lo studio parametrico svolto, evidenzia la notevole influenza dell'umidità sulla stima dell' ETC, e quindi la necessità di svolgere una simulazione igrotermica per la valutazione di questo parametro.

1 Introduction and Motivation

Heat and mass transfer in porous material is a subject of great interest for a wide range of engineering applications, from drying processes to fuel cell design , most of which are related to high energy consumption.

An accurate calculation of heat and mass distribution is therefore required in order to lower energy consumption and optimize industrial processes. We can speak of heat and moisture transfer in those problems in which we are mainly interested in the transport of water inside a porous media . A list of heat and moisture transfer applications, which is by no means exhaustive can include among others: oil extraction, drying of wood, food, granular materials and fabrics,pollutants infiltration, heat exchangers, transport in composite membrane and thermal insulation.

For what concerns building physics, the combined heat, air and moisture transfer in building elements is of paramount importance for accurate energy consumption prediction, thermal comfort evaluation, mould growth risk assessment and material deterioration analysis.

Humidity can affect energy consumptions increasing both heating and cooling energy demand. During winter, the presence of humidity in the external walls can significantly reduce thermal insulation of a building [21, 16], leading to increasing heat losses and to extra energy consumption. During summer, energy demand is influenced by the amount of water condensing inside the first layer of internal walls. In most of the cases latent heat of condensation represent a large amount of the overall cooling energy demand [62]. It is possible to reduce cooling and heating energy consumption through moisture buffering provided by the use of hygroscopic materials inside the building [47].

The presence of water inside building components can leads to mould growth. In particular, if the surface moisture on internal walls reaches an equilibrium moisture of 80%, mould formation can be expected [3]. This is an important hygienic issue, since the presence of mould can have a detrimental effect on the healt of the occupants.

Among the problems caused by the presence of water inside building material, structural damage is the most important in terms of economic impact. Corrosion and material deterioration caused by moisture runs into billions in Germany alone every year [33]. A list of failure caused by humidity , and the ones that can be detected through hygrothermal simulations can be found in [42]. Structural damaged due to humidity is very common in historical buildings, because they have been exposed to the effect of water for a long time. Moreover, for historical buildings an external insulation is not always possible, since the exterior appearance of the facade has to be mainteined. This result in placing the required insulation in the interior of the building, which can reduce the overall drying potential of the wall, leading to internal condensation. In such a situation a high quality energy retrofit must be studied, in order to guarantee a long term preservation of the building.

Numerical simulation can supply important information for a correct design and the choice of proper materials; however a realistic modeling may present

high complexity.

The vast majority of building physics hygrothermal applications concerns interaction between a porous and a fluid media. The flow field requires a finer discretization of the domain to be solved appropriately, especially in the case of development of turbulence, and this results in a high increase of computational effort and simulation time. For those reasons, the effect of the fluid flow is often taken in account through the use of convective transfer coefficients (CTCs). It has been shown anyway, that this simplification can leads to errors in mass and tempertature distribution [14]. This is the reason of the increasing interest among researchers in modeling heat and mass transfer using a conjugate approach.

A conjugate approach does not require to choose a CTCs to be applied at the porous media boundary conditions, since the mass flux and heat flux are directly calculated during the simulation, resolving the balance equations for the fluid media. Even if many authors have studied the subject, very often the balance equations are resolved using constant CTCs.

During this decade a large number of heat, air and moisture (HAM) transfer simulation tools have been created by researchers to investigate particular problems concerning energy efficiency and material preservation.

Two of the most known available commercial HAM softwares exhibit a lack in 3D and CFD modeling. This fact undergoes them to a big constraint in the cases that can be studied with these softwares.

The first part of this work concerns the study and development of a general and flexible model for hygrothermal analysis. In order to do so, a coupled approach is followed, since no previous knowledge of the CTCs is needed.

On the one hand, this approach allows the simulation of a larger number of problems. On the other hand this approach requires great computational effort if applyed to building physics problems.

This can be explained considering some common characteristics in building physics hygrothermal simulations:

1. *Time dependent simulations*: in hygrothermal simulations, boundary conditions like temperature and humidity, are typically time dependent. This imply that the simulations have to be time-dependent, since steady state conditions are not reached. Even in the case of constant boundary conditions, a time dependent simulation is likely to be the subject of the study, since in most of the study the focus is on the dynamic behavior of porous materials, e.g.: investigation of dry time.

2. *Long period simulations*: moisture transfer diffusive coefficients are in general several order of magnitude smaller than the energy transfer diffusive coefficients, as shown in 5.3.3. For this reason, humidity transport equation presents greater time constant. This means that the effect of humidity boundary conditions takes a longer time to be transported inside the porous domain than temperature boundary conditions. Long period simulations are therefore required in order to see the dynamic behavior of

porous material. Moreover, longer simulations, typically in order of years, are often necessary, when the purpose of the study is to investigate water accumulation inside building materials, which is often the case.

3. *Parametric study*: results of numerical simulations are highly dependent on boundary conditions and material properties. In the vast majority of building physics studies, is common practice to carry on sensitivity studies and parametric studies, investigating the influences in the solution.

Taking into account these considerations, avoiding a coupling approach can be convenient in terms of computational time. This is surely the case of retrofitting of ancient buildings. One of the most critical elements in energy retrofitting, are the structural elements, which can be severely damaged by high contents of moisture over a prolonged period of time. Thermal bridges represent a critical case (e.g: timber beams when an internal insulation has been applied). For this reason the second part of this thesis introduce a simplified approach that can be applied in the case of air cavities between the wall and the beam ends.

2 Modeling of heat and moisture transfer in porous materials

In this chapter a brief explanation of the physical mechanisms of heat and moisture transfer in porous materials and air is exposed. The physics of heat and mass transfer in porous media has been largely studied in the last century, and a review of the most widely used methods is presented. Despite being a relatively recent approach, the conjugate model have been the subject of a great number of publications in the last few decades. This was possible mainly due to both the increase in computational power and to the optimization of computational fluid dynamics algorithms. A brief overview of the methods proposed by various authors for taking into account the effect of a fluid flow over the heat and mass transfer in a porous media is presented at the end of the chapter.

2.1 Modeling approaches: state of the art

Most of the building materials are porous media. One of the first analysis of moisture transfer in porous media, was a work by Lewis [37], and the idea that drying was essentially a diffusion problem was lately picked up by Sherwood [53, 52]. These first works were based on the idea that water transfer was well described by a diffusion equation, in the form of:

$$\frac{\partial C_m}{\partial t} = D\nabla^2 C_m \tag{2.1}$$

where C_m represents the moisture content and D was a experimentally determined parameter. Neither the capillary transport nor the diffusion in the vapour phase was considered to be significant. Later works pointed out how the water transfer was strictly influenced by surface tension forces, resulting in a transport due to capillary action [51, 15]. On the basis of these works, other authors [22] studied the limitations that apply to a description of water transfer based on equation 2.1.

When a certain amount of water is present inside a porous material, it can move inside the porous structure by means of several different transportation mechanisms, which will be later analyzed. Along with mass transport, moving water cause a heat transport inside the material, through his enthalpy. This means that the equations of heat and mass transfer are strongly coupled.

Krischer was the first author to consider the influence of energy transport in drying processes non negligible [30]. Phillip and DeVries included capillary water transport, vapour and energy transport into the governing equations that described their model of drying process [50]. Similar equations was derived by Luikov [38], using an approach based on irreversible thermodynamics. Using volume-averaging and the mass and energy balance equations for a continuous media, assuming local thermal equilibrium, Whitaker derived a similar system of equations [64].

From these models, many others were developed, great part of which are based on the following approach:

- *Macroscopic models*: this approach is based on balance equations applied to a macroscopic region. The material is considered to be homogeneous, and its properties isotropic. Two main different approach exist: 1) *phenomenological approach*: is based on the driving forces of transport, that is, the potentials that cause the water transport inside the porous body. The models from Phillip and DeVries and Luikov belongs to this category, as well as WUFI and Delphine. 2) *averaging or continuum model approach*: this is basically the approach used by Whitaker. Since at the microscopic scale the complex pore structure is involved, a description of the transport mechanisms based on the microscopic level remains rather difficult. Nevertheless, some authors take this level as a starting point for the description of the heat and moisture transfer mechanisms [7]. The microscopic balance equations are written for a representative elementary volume (REV) and the macroscopic balance equations are derived through volume-averaging. The major advantage of the continuum model approach is that for large enough volume of the REV, the property of the porous body can be considered constant in space. In fact, for big REV, the averaged properties of the REV approaches the mean properties of the corresponding homogeneous porous material. This means that there is a minimum dimension of the REV which permits to obtain meaningful results. This dimension is strictly related to the mean pore dimension in the material. Assuming an average pore dimension of 10^{-5} the spatial resolution of the model should be bigger than 1mm [45]. Some authors have shown how the transport equations derived by this two approaches are essentially the same [9]. The averaging technique gives anyway more insight in the required assumptions.

- *Pore-network models*: they take the microscopic structure into account, representing the material as a network of pores. They use micro tomography images to extract the pore network. This kind of approach is mainly use to determine the transport properties of the porous materials. An historical overview can be found in [8]

A more detailed classification of the heat and moisture transfer methods in porous materials can be found in [14].

2.2 Moisture storage in porous materials

Building materials like concrete, bricks, sandstone, are hygroscopic and capillary active. This means that if they are in presence of moist air, they absorb water until reaching an equilibrium with the humidity of surrounding air, and if they are in contact with liquid air, they will pick up water by the action of capillary forces.

Inside porous materials, the chemical equilibrium between air and liquid water is modified by the presence of viscous forces inside the capillary. Considering humid water as an ideal mixing, the chemical equilibrium between air and liquid water can be described, applying the laws of thermodynamics, as:

$$y_w p = p_s(T) \exp\left(\frac{x_w(p_w - p)}{RT}\right) \tag{2.2}$$

also known as Kelvin's formula. In equation 2.2, y_w is the molar fraction of liquid water in air, $p_s(T)$ is the saturation pressure at the given temperature, x_w is the molar volume of liquid water, R is the universal gas constant, and p_w is the water pressure. If the interface between water and air has no curvature, p_w is equal to p, and equation 2.2 simplifies into the well known Raoult's law. Inside a capillary, viscous forces cause a curvature of the water-air interface. Doing a balance of the various forces, assuming a spherical meniscus as in figure 1 , we can see that a difference between the water pressure p_w right over the meniscus and the air pressure is created:

$$p\pi r_c^2 = p_w \phi r_c^2 + 2\pi r_c \sigma cos(\theta_c) \tag{2.3}$$

$$p - p_w = \frac{2\sigma cos(\theta_c)}{r_c} \tag{2.4}$$

where σ is the water surface tension, θ_c is the contact angle between the meniscus and the capillary wall, and r_c in the radius of the capillary.

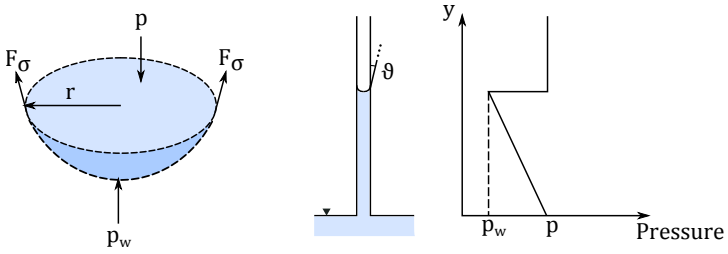

Figure 1: Balance of forces over a meniscus, and values of pressure along a vertical capillary.

If we define the capillary pressure p_c as: $p_c = p - p_w$, we can rewrite equation 2.2 as

$$\varphi = exp\left(-\frac{P_c}{\rho_w R_v T}\right) \tag{2.5}$$

where φ is the relative humidity, ρ_w is the water density and R_v is the gas constant of water vapour. The porous material can be thought as a network of interconnecting pores, where the water is free to move freely. In particular, when equilibrium is being reached, water will flow from bigger pore to the smallest one, due to the greater suction pressure. Thus, combining now equation 2.5

with 2.4, we can find the values of the radius up to with the capillary are filled with water, under equilibrium assumption:

$$r_c = -\frac{2\sigma cos(\theta_c)}{\rho_w R_v T ln(\varphi)} \tag{2.6}$$

This means that, if the porous material is surrounded by air with a given value of relative humidity, we can expect that all the pores with radius smaller than the value given by equation 2.6, will be filled with water if equilibrium is reached. In figure 2, the relation between porous radii and relative humidity is shown, assuming contact angle $\theta_c \approx 0$.

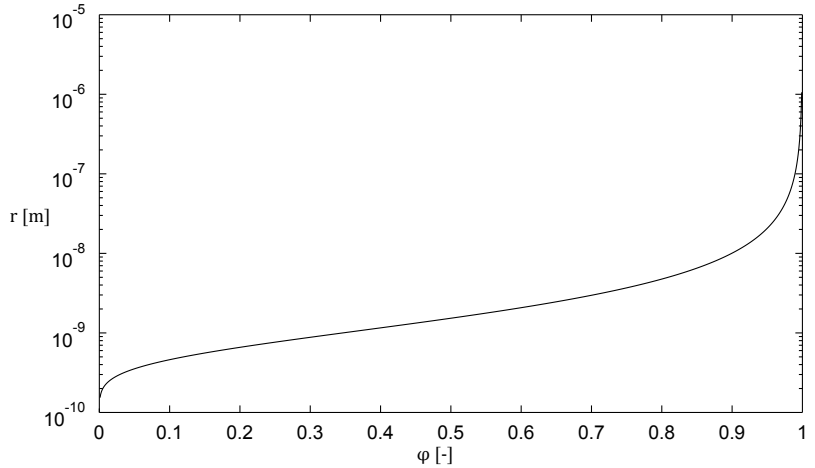

Figure 2: The figure shows the radius up to with the pores are filled with water, under equilibrium assumption, for increasing values of relative humidity. The radius value is plotted in logarithmic scale.

As we can see, for values of relative humidity higher than 0.95, the curve becomes steep. Figure 2 can be used to explain the relation between water content in porous material and relative humidity. The curve that gives the total water content iside a porous material with respect to the relative humidity, is called water retention curve, or water storage function. This curve is shown in figure 3. In the last part of the water storage function, the content of water inside the porous material increases steeply with respect to the relative humidity. Assuming the validity of capillary model, this can be explained through the filling of pores with increasingly bigger radii, which has been shown to have a similar behavior in figure 2. Therefore, even if the water storage function is highly material specific, and is always obtained through experimental measurements, we can expect a common behavior in the last part of the curve for all porous materials.

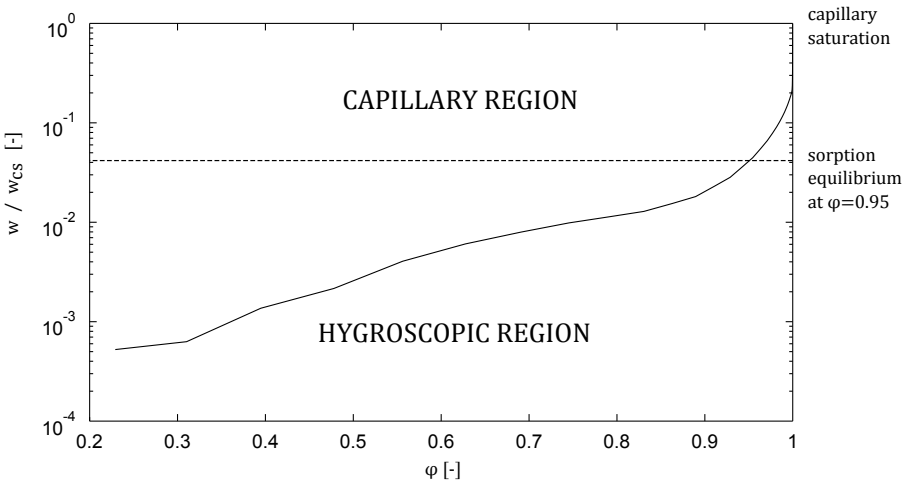

Figure 3: Water storage function for a brick. On the y axes the water content normalized with respect to the water content at capillary saturation, on a logarithmic scale, is plotted. The two main regions of interest for building physics simulations are plotted.

The main mechanisms of transport of vapour and liquid water inside a hygroscopic and capillary active porous material, can be divided on the base of the range of relative humidity values in which they are predominant.

In particular, for building physics applications, two regions of interest can be described.

1) *Hygroscopic region*: this region is characterized by vapour diffusion and effusion transport (see chapter 2.3.2) . The vapour can condense inside the porous surface, creating a water film directly above the pore surface. This film is initially monomolecular up to a value of φ of 15% [31], and with rising values of relative humidity becomes increasingly thick. As the water layer grows, onset of liquid transport take place, through surface diffusion. In this region capillary transport is also present, but it does not play a major role in the total water transport.

2) *Capillary water region or super-hygroscopic region*: as the relative humidity increases, pores are filled with water. At a value of relative humidity above 95% capillary transport becomes predominant over vapour diffusion transport. The water content can increase until reaching its maximum value at capillary saturation condition, w_{cs}, which is the water content at the equilibrium when the porous material is wetted by liquid water. In this condition, some air is still trapped inside the pores of the material.

When a water content equal to w_{cs} is reached, no more water transport is possible inside the porous material. The only way to increase the water content is to replace the trapped air with water. This can be done through suction under pressure [33], as done in mercury porosimetry [31], or applying temperature

gradient. This will increase the water content, reaching the maximum saturation possible. Since this situation is practically unlikely in almost building physics case of study, this thesis will consider the capillary saturation water content w_{cs} as the maximum water content possible.

The water storage function is determined experimentally. Two different experimental procedures must be used for hygroscopic region and capillary water region [31]: the first part of the curve is usually obtained with a universally used procedure. A porous material specimen is placed in environment regulated by means of salt solutions and the content of water at the equilibrium is calculated by weighing it. The relative humidity is regulated using different concentrations of salts in the solution, up to a value of 95% relative humidity. In this region the curve become very steep, and the use of this kind of procedure would lead to very inaccurate results. In the super-hygroscopic region different methods must be used, such as mercury porosimetry or centrifugal tests. One of the most accurate is the use of a pressure plate, in which suction pressure is controlled, and the water content is determined after reaching of equilibrium. Than, through equation 2.5, it is possible to calculate the relation between φ and the water content w. Despite the use of two different analytic methods, the curves present no discontinuity or derivative change for the value of φ in which the method of inspection is changed. The fact that the water retention curve as a function of φ is continuous and has a continue first derivative, tells that φ can be used as a true potential over both the hygroscopic and the capillary water regions [33, 31]. Moreover, capillary pressure p_c does not play any role in water transport in non capillary-active materials , thus there would be no physical meaning in using it as potential.

In the range of 20 to 70 $°C$ the influence of temperature over the water retention curve can be disregarded [33]. The moisture retention curve can present hysteresis phenomena. This hysteresis behavior, firstly explained by means of capillary transport in [40], was implemented in the study some authors [56], based on the model developed in[43]. In most building materials anyway, the hysteresis between absorption and desorption isotherms is not remarkable, and when it is, a sufficient accurate result can be obtained averaging the absorption and desorption curve [33]. In the case of gypsum, it has been shown that the influence of including hysteresis is not as large as the influence of the uncertainty of sorption and vapour permeability [24].

2.3 Mechanisms of water transport in porous materials

The various mechanism of water transfer that can occur in the porous material are listed in table 1. Some of these transport mechanisms can be safely disregarded for most building physics studies. This is the case of electrokinesis and seepage flow [33]. In this thesis liquid and vapour transfer caused by a gradient of total gas pressure won't be considered, since the differences in total pressure (equal to the atmospheric pressure) over the porous bodies are considered to be negligible. Moreover, the gaseous permeability is much higher than the liquid permeability, resulting in a quick equalization of possible pressure differences

in the gaseous phase [13]. Thermodiffusion, also known as Soret effect, can be disregarded for temperatures below $50°C$ [59, 33].

Table 1: Mechanisms of water transport that can occur inside a porous material and the relative driving potentials.

LIQUID	TRANSPORT
MECHANISM	POTENTIAL
capillary conductivity	capillary pressure
surface diffusion	relative humidity
hydraulic flow	total pressure
seepage flow	quote
electrokinesis	electric potential

GASEOUS	TRANSPORT
MECHANISM	POTENTIAL
vapour diffusion	vapour density
vapour effusion	vapour density
thermodiffusion	temperature
gas flow	total pressure

2.3.1 Capillary conduction and surface diffusion

Capillary transport was historically taken into account using water content as potential, of the form

$$J^c = -D_w(w)\nabla w \tag{2.7}$$

where w is the water content. Even if this choice can lead to good approximations of the physical process, the coefficient $D_w(w)$ depends strongly on the boundary conditions [33]. A more physically meaningful relation can be found using the Hagen-Poiseuille equation describing the liquid flow through a cylindrical pore under assumption of Newtonian laminar flow

$$J^c(r) = -\frac{\pi r^4}{8\nu_w}\frac{\partial p_c}{\partial x} \tag{2.8}$$

where ν_w is the dynamic viscosity of the fluid. Through pressure plate or mercury porosimetry tests and the use of equation 2.4 it is possible to find the correlation between the liquid volume and the pore size. Assuming that the length of the pores is only dependent on the dimension of the radius, the number of the pores with a given radius $f(r)$, also known as pore size distribution, can be obtained. Assuming that all capillaries are parallels, multiplying equation 2.8 with $f(r)$ and integrating for the radius, it is possible to obtain the total capillary flow, in the form of

$$J^c = K_l \nabla p_c \tag{2.9}$$

where K_l is the capillary conductivity. Equation 2.9 takes the form of Darcy's equation of hydraulic flows. Since the real geometry of the pores can

be different from the assumed one, correction through comparison with the experimental results of the capillary conductivity must be applied. Moreover, for a certain value of relative humidity, capillary conduction and surface diffusion can coexist. Surface diffusion is the transport of liquid water that occur inside a condensate film over the porous surface. While surface diffusion take place into those pore that are not jet saturated, for a certain value of φ, capillary conduction can be present in smaller pores, according to 2.6. Since the two mechanisms take place simultaneously, they can only be measured simultaneously. The coefficient K_l is further modified to take surface diffusion into account. The capillary conductivity can be considered a function of the relative humidity. This function is obtained by means of experiments and is material-specific.

2.3.2 Vapour diffusion and vapour effusion

These two mechanisms of water transfer are strictly related. Vapour diffusion is the transport of vapour due to a gradient of vapour partial pressure. Thermodiffusion, also known as Soret effect, is the vapour transport due to a temperature gradient. Both can be described by the Fick's law of diffusion. According to [23], Fick's law of diffusion for water vapour in air can be written as

$$J^d = -\rho_g D_{av} \nabla m_v \tag{2.10}$$

where D_{av} is the binary diffusion coefficient of water vapour in air, ρ_g is the total density of the gas phase and m_v is the vapour mass fraction, equal to

$$m_v = \frac{\rho_v}{\rho_g} \tag{2.11}$$

where ρ_v is the vapour density. Writing the Fick's law in terms of densities is only valid if the total density of the gaseous phase ρ_g is constant [6]. This can be safely assumed for temperatures under $50°C$ [13]. Combining equations 2.10 and 2.11, we obtain

$$J^d = -D_{av} \nabla \rho_v \tag{2.12}$$

.

When diffusion inside a porous material is considered, additional resistance to the diffusion must be taken into account. This resistance is due to pore tortuosity, pore obstruction by water capillary condensation and open porosity of the material. This is done introducing the resistance factor of the porous material μ. The resulting equation becomes

$$J_v^d = -\frac{D_{av}}{\mu} \nabla \rho_v \tag{2.13}$$

where J_v^d is the diffusive flux of water vapour.

Together with vapour diffusion, vapour effusion can occur. Vapour diffusion, or Knudsen diffusion, occurs when the collisions between vapour molecules and the pore wall are more frequent than the collisions between themselves. This

effect can be taken into account using the density gradient as driving potential. Even if the dependence from pressure and temperature of this effect are different from the dependencies of vapour diffusion in porous material, in building physics vapour effusion is considered adjusting the resistance factor μ. In this thesis μ is considered to be function of the relative humidity. This function is obtained by means of experiments and is material-specific.

In figure 2.3.2 is shown how these processes can coexist in various ranges of relative humidity. In figure 2.3.2 a, vapour diffusion transfers water vapour accordingly to vapour density gradient, while surface diffusion moves liquid water by means of capillary suction pressure. If relative humidity increase, the capillary can be saturated with liquid water. In figure 2.3.2 b, vapour diffusion is not present anymore, and capillary transport take place. According to equation 2.6, for increasing values of φ up to 1, the maximum value of the radius of capillaries that are saturated under equilibrium condition increases. In figure 2.3.2 c an external suction pressure have been applied, until all capillaries are completely saturated.

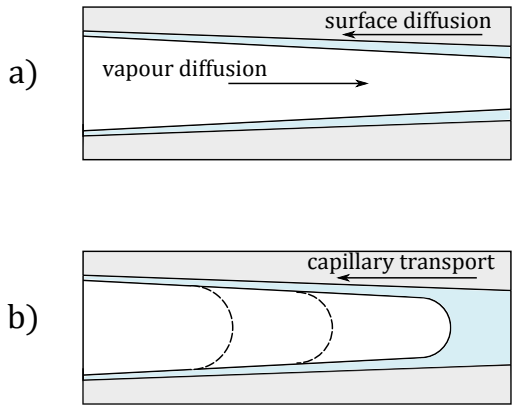

Figure 4: Mechanisms of water transfer in capillary pores for increasing values of relative humidity a) Vapour diffusion and surface diffusion b) Capillary transport, with position of the meniscus for increasing values of relative humidity up to 1, when no more water transport is observed [33].

2.4 Mechanisms of heat transport in porous materials

In table 2 the mechanisms of heat transport in porous material are listed. The air enthalpy flow is not considered due to the previous assumption of constant value of total pressure. The remaining mechanisms of water and heat transport will be now briefly explained.

Table 2: Mechanisms of heat transport that can occur inside a porous material and the relative driving potentials.

HEAT	TRANSPORT
MECHANISM	POTENTIAL
conduction	temperature
radiation	4th power of temperature
water enthalpy flows	capillary pressure, vapour density
air enthalpy flows	total pressure

2.4.1 Heat conduction and radiation

The conductive heat flux in the porous media can be described by Fourier's law:

$$q^c = k_{eff} \nabla T \tag{2.14}$$

where k_{eff} is the effective thermal conductivity. The effective thermal conductivity should be obtained through volume average, as in [64]. Anyway, the thermal conductivity of the porous material is influenced mainly by the water content. Thus it is possible to consider k_{eff} as function of the water content, as in [13].

When the porous material is dry, the effective thermal conductivity is equal to the thermal conductivity of the dry porous solid matrix, k_s. Since k_s is determined experimentally applying a measured heat flux to a specimen of the porous material and monitoring the temperature on both sides of the specimen, the effect of internal radition is included in k_s. This influence depends on the temperature. Anyway, since the temperature investigated in this thesis are all below $40°C$, this dependence is not considered.

2.4.2 Enthalpy flows

The water and air enthalpy flows are taken into account multiplying the air flux and the water flux for their specific enthalpies:

$$q^e = J_g h_g + J_l h_l \tag{2.15}$$

where J_g and J_l are the total gas flux and the liquid flux inside the porous media. We can further simplify this considering negligible the total enthalpy transferred by air. This can be done considering that we have assumed a negligible total pressure gradient over the porous domain, and that the specific enthalpies of liquid water and vapour are big compered with the specific enthalpy of air. We can write

$$q^e = J_v h_v + J_l h_l \tag{2.16}$$

where

$$h_v = c_{p,v} T + H_{ev}$$

and

$$h_l = c_{p,l} T$$

.

The complete system of energy and mass balance equations for the porous material, and the assumptions made, are explained in appendix 4.2.

3 Considerations on turbulent flow

The Navier-Stokes equation for incompressible flow describe correctly the behavior of the fluid in both the laminar and turbulent regime. Anyway, if the flux becomes turbulent, random fluctuations start to occur in the velocity field. These fluctuations generate instability in the flow. Even if the original laminar flow presented a two dimensional nature, turbulent fluctuations give to the flow a more complex three dimensional spatial character. The fluctuations generate the so-called turbulent eddies, which are coherent structures with a wide range of length scale. The smallest vortices cause a energy dissipation inside the flow, transferring kinetic energy into thermal energy. In particular, when the characteristic Reynolds number for small eddies approach unity, that means that viscous forces have the same strength of inertial effects, the vorteces reaches their maximum dissipation capabilities. At this scale, also called the Kolmogorov's scale [39], the lenght of these small vortices can be correlated to the dimension of the big eddies through an order of magnitude estimate:

$$\eta \approx L_0 Re_l^{-3/4} \tag{3.1}$$

where η is the scale of the small eddies, L_0 is the scale of the big eddies and Re_l is the Reynolds number for the problem. Considering a typical Reynolds number of 10^5, the ratio of η/L_0 assume a value with an order of magnitude of 10^{-4}. Thus, for typical flow problems, a very high spatial resolution would be necessary in order to see the actual scale in which energy dissipation occurs. This approach of solving the Navier-Stokes equations is called direct numerical simulation DNS, and can be practically realizable only in small domains. A more computationally economical is to model the dissipation phenomena that occurs under a certain scale length. The most used approach is doing a Raynolds average of the Navier-Stokes equations (RANS). This method uses the Reynolds decomposition to split the velocity components into a steady mean value V, and in a component that represents the statistical fluctuations v'

$$\mathbf{v}(t) = \mathbf{V} + \mathbf{v}'(\mathbf{t}) \tag{3.2}$$

For steady mean flow, time average is defined as

$$\mathbf{V} = \int_0^{\Delta t} \mathbf{v}(t)\, \mathrm{d}t \tag{3.3}$$

where Δt is a period of time bigger than the one associated with the slowest variations of the flow properties. For time-dependent flows, the time-average is replaced by the so called 'esemble average, that is defined as the average of the instantaneous value over a big number of repeated identical simulations [39]

$$\mathbf{V} = \lim_{n\to\infty} \frac{\sum_1^n \mathbf{v_n}(\mathbf{x}, t)}{n} \tag{3.4}$$

This averaging process modify the Navier-Stokes equation, resulting in the Reynolds averaged Navier-Stokes equation:

$$\frac{\partial(\rho_g \mathbf{V_g})}{\partial t} + \nabla \cdot (\rho_g \mathbf{V_g} \otimes \mathbf{V_g}) = \nabla \cdot (-\mathbf{pI} + \mu \nabla \mathbf{V_g}) - \nabla \cdot (\rho_\mathbf{g} \overline{\mathbf{v_g}' \otimes \mathbf{v_g}'}) + \mathbf{g}\rho_\mathbf{g} \quad (3.5)$$

where $\rho_g \overline{\mathbf{v_g}' \otimes \mathbf{v_g}'}$ are the so called Reynolds stresses, or turbulent shear stresses, caused by the enhanced momentum exchange due to turbulence.

These additional stresses must be modeled, on the basis of some assumptions, like the isotropy of the turbulent kinetic energy. Various closure models are available in the literature, most of which uses more than one additional transport equation to obtain the local Reynolds stresses. Even if in the current thesis all the flow regime have been chosen to be laminar, turbulent flow can be easily taken into account through the built-in CFD modules in COMSOL Multiphysics. At the moment, the Spalart-Allmaras, $k-\epsilon$, $k-\omega$ and Low Reynolds number $k-\epsilon$ are available. Nevertheless, some considerations must be done about the models.

In figure 5, the development of the velocity and thermal boundary layer are shown along a vertical plate. Since in this case T_w is higher than T_∞ and no heat transfer mechanisms are considered other than convection, the solid is being cooled, and the heat flux is directed as the normal to the surface. The heat transfer can be considered through a heat transfer coefficient, α, as in equation

$$q_w = \alpha \left(T_w(y) - T\infty \right) \quad (3.6)$$

This convective heat transfer coefficient (CHTC) is normally obtained through experimental correlations, or in some cases, through the heat and momentum transfer analogy and analytically solving the velocity boundary layer equations. Even if CHTCs are used in great part of building physics analysis, it is not always possible to find in literature a CHTC for the specific geometry and boundary conditions that are being considered.

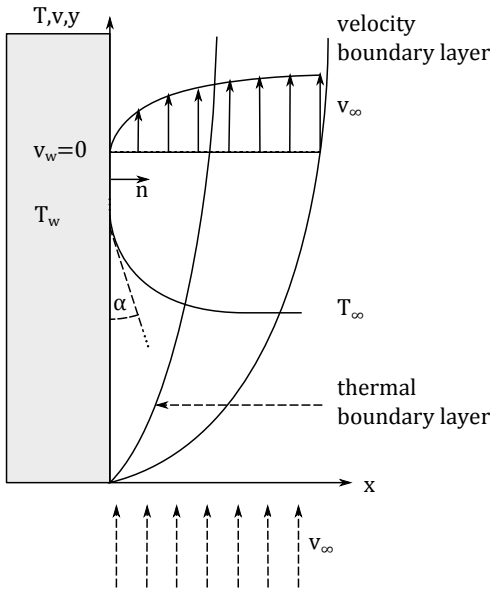

Figure 5: Development of the velocity and thermal boundary layers along a vertical plate. The heat flux can be found knowing that $tg(\alpha) = \partial T/\partial x$

Another way to obtain the heat flux at the interface is by resolving directly the velocity and thermal boundary layers, in a numerical simulation. In almost all practical cases, the no-slip condition on velocity field can be assumed, namely

$$\mathbf{v}|_{x=0} = 0 \tag{3.7}$$

This means that heat transfer in the fluid media occurs only due to conduction. The heat flux at the wall can thus be expressed with Fourier's law

$$q_w = -k\frac{\partial T}{\partial x}\bigg|_{x=0} = tg(\alpha) \tag{3.8}$$

This means that the an error in the computation of the temperature derivatives at the wall will directly influence the heat transfer. For minimizing the error on the heat flux, a good spatial resolution is requested in the fluid domain near the wall. While this request can be easily accomplished for a laminar flow, it is far more problematic for a turbulent flow. In the $k-\epsilon$ and $k-\omega$ closure models, the velocity and thermal boundary layers are modeled through the use of the standard wall functions [2]. These are analytical expressions, which are derived for equilibrium boundary layers, and will therefore produce less accurate results for complex flows and should be avoided when the main purpose is to study the heat flux at the wall [44]. In this situation, the Low Reynolds number $k-\epsilon$ model should be used, which resolve directly the boundary layers, providing a good enough spatial resolution in the proximity of the wall. This

model could not always be feasible for the study of complete building geometry, due to the increase of computational costs, as shown in [13].

4 Mathematical model

4.1 Coupling approaches: state of the art

In almost all hygrothermal simulations, the influence of a fluid media, commonly humid air, over heat and moisture transfer must be taken into account. For doing this, several different approaches exist, which couple the equations of heat and moisture transfer in porous media with the transport equations of air. The most common are here described:

- *Non-conjugate*: convective transfer coefficients (CTCs) are used. CTCs account for heat and moisture transfer in a simplified way, for different reasons. CTCs are often estimated through experiments that uses very simplified geometry, but heat and mass transfer are highly dependent on the geometry of the problem, so their use for geometry other than the one used during their computation is not recommended. Often convective mass transfer coefficients are derived from the convective heat transfer coefficients through the Cilton-Colburn analogy [23], which can not always be applied (namely, no radiation must be present, no coupling between and mass transfer, analogous boundary conditions). Moreover, the temporal and spatial variation of CTCs is often not taken into account.

- *Semi-conjugate*: the spatial or temporal variations of the CTCs is taken into account. The spatial variation can be considered if the CTCs are obtained analytically, solving the boundary layer equations, and applying the heat and momentum transfer analogy, which relates velocity gradients to thermal gradients. Another method is to determine the CTCs with a CFD simulation, and apply them later on the porous domain [29]. The temporal variation of the CTCs can be applied considering the CTCs dependence on temperature and concentration [48]

- *Conjugate*: the heat and moisture transfer in the porous material is computed simultaneously with the equations of heat and mass transfer in the fluid media. In this way it is possible to compute the solution avoiding the previous knowledge of the CTCs. In some cases of forced convection, it is possible to consider the flow field as quasi steady-state, computing in a transient way only the equations of heat and mass transfer but not the momentum equation. In other cases, also the momentum equation must be computed simultaneously.

An accurate review of heat and mass transfer modeling at air-porous material interfaces can be found in [14].

4.2 Conjugate model balance equations

In this thesis a continuum approach is used in order to find the mass and energy balance equations, as done in [45, 64, 13]. A porous media is a combination of

three different phases, liquid, gaseous and solid. Representing the actual geometry of the pores, and phases interfaces on a microscopic level is not possible when operating at the scale of typical building physics problems. In this case it is advantageous to use a homogenization technique on a representative portion of the porous material, in order to describe the phases distributions on the basis of averaged microscopic properties. To do this, it is necessary to operate at a scale between the mesoscopic and the macroscopic scale. The mesoscopic scale is the scale where the separations of the different phases can be distinguished clearly, but their properties appear as homogeneous. At the macroscopic scale, the separations of different phases can not be distinguished anymore. The representative elementary volume represented in figure 4.2, or REV, must be big enough to avoid spatial oscillations of material properties [45], but small enough to ignore the macroscopic variations in the material, e.g. brick separations, macro cracks. As already mentioned, the dimension of the REV are strictly related to the maximum dimension of the pore in the material considered. In general, the REV should be one or two order of magnitude larger than this value. For most common porous material this means that the REV should be large at least 10^{-3}m [45].

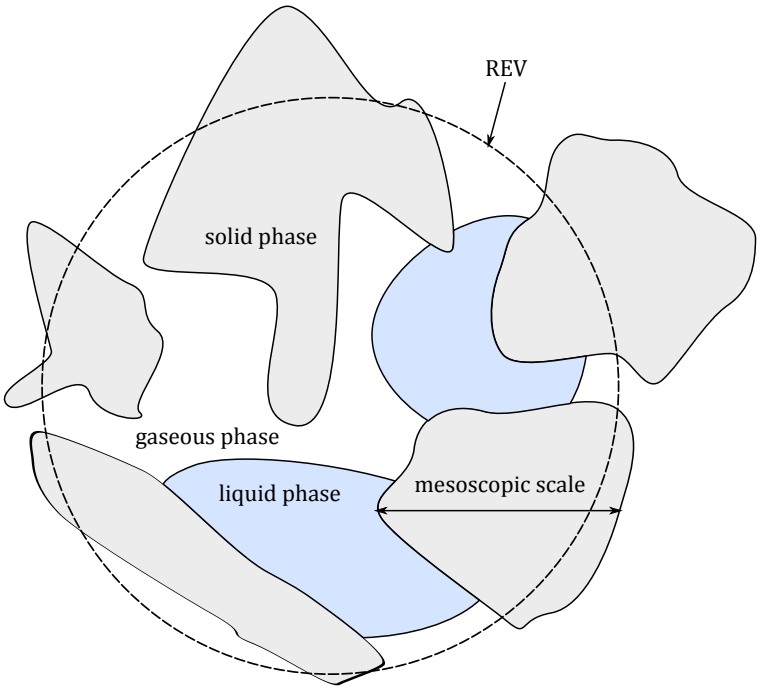

Figure 6: Representative elementary volume. The different phase interfaces can be distinguished, but the material properties can be assumed as homogeneous, since no macroscopic variations of the geometry are present.

The averaging process results in the need of using phase contents instead of phase densities in the balance equations. While phase densities ρ_i are given in $\left[\frac{kg}{m_i^3}\right]$, where m_i^3 denote the volume of the ith phase, phase contents w_i are given in $\left[\frac{kg}{m_{pm}^3}\right]$, where m_{pm}^3 is the volume of the porous material. Denoting with ϕ the material porosity, and with ϕ_l the porosity occupied by liquid water, the phase content for the solid, liquid water, air and vapour can be written as:

$$w_s = (1-\phi)\rho_s \tag{4.1}$$

$$w_l = \phi_l \rho_l \tag{4.2}$$

$$w_a = (\phi - \phi_l)\rho_a \tag{4.3}$$

$$w_v = (\phi - \phi_l)\rho_v \tag{4.4}$$

Where ρ_s is the density of the solid matrix. We can further simplify these relations, considering that the mass contribution of the vapour is negligible with respect to the liquid water content. Under this assumption, the total water content $w\left[\frac{kg_w}{m_{pm}^3}\right]$, defined as

$$w = w_l + w_v$$

results equal to w_l. Thus, using equation 4.2, we can find that ϕ_l can be written as

$$\phi_l = \frac{w}{\rho_l} \tag{4.5}$$

Moreover, ϕ can be considered equal to the volume occupied by liquid water at capillary saturation, w_{cs}.

The general balance equations for the porous media are obtained as in [13], doing the following assumptions:

1. Air, liquid and solid material matrix are assumed incompressible.
2. Pressure variations are small so they do not affect thermodynamic properties.
3. Local thermal equilibrium between the phases is assumed.
4. Potential and kinetic energy changes are assumed to be small compared to thermal energy changes and are neglected in the gaseous phase.
5. Pressure work and viscous heating/dissipation are neglected.
6. Heat source terms other than evaporation or condensation of liquid water are not taken into account.

4.2.1 Mass balance in porous media

The mass balance for the ith phase can be written as:

$$\frac{\partial w_i}{\partial t} = -\nabla \cdot (J_i) + \sum_j \frac{\partial w_{i,j}}{\partial t} \tag{4.6}$$

where $w_{i,j}$ is the mass exchanged between the ith and the jth phase. Since no chemical reactions are considered, is evident that

$$\sum_i \sum_j \frac{\partial w_{i,j}}{\partial t} = 0 \tag{4.7}$$

In a hygrothermal simulation we are interested only in the mass balance for the water content. We can sum the liquid and vapour phase mass balances to obtain the total water balance inside porous media:

$$\frac{\partial (w_l + w_v)}{\partial t} = \frac{\partial w}{\partial t} = -\nabla \cdot (J_v + J_l) + \frac{\partial w_{w,v}}{\partial t} + \frac{\partial w_{v,w}}{\partial t} \tag{4.8}$$

where $w \left[\frac{kg}{m^3_{pm}}\right]$ is the water content, J_v is the vapour flux and J_l is the liquid flux.

Using equation 4.7, equation 4.9 can be written as

$$\frac{\partial (w_l + w_v)}{\partial t} = \frac{\partial w}{\partial t} = -\nabla \cdot (J_v + J_l) \tag{4.9}$$

4.2.2 Energy balance in porous media

The energy balance for porous media can be written as:

$$\frac{\partial H_{pm}}{\partial t} = -\nabla \cdot (J_v h_v + J_l h_l + q^c) \tag{4.10}$$

Where $H_{pm} \left[\frac{kJ}{m^3_{pm}}\right]$is the total enthalpy of the porous media, q^c is the conductive heat flux,h_v and h_l are the vapour and liquid water enthalpies, in $\left[\frac{kJ}{kg}\right]$.

The total enthalpy can be written as the sum of the enthalpies of the various phases:

$$H_{pm} = h_s w_s + h_l w_l + h_a w_a + h_v w_v \tag{4.11}$$

where h_s is the enthalpy of the solid matrix expressed in $\left[\frac{kJ}{kg}\right]$. Consider that w_s is function of ρ_s, which is usually an unknown property of the porous material. The density of the dry porous material, $\rho_m \left[\frac{kg}{kg_{pm}}\right]$, can be defined as

$$\rho_m = (1 - \phi)\rho_s + \phi\rho_a \tag{4.12}$$

The specific enthalpy h_m of the dry porous material is the weighted average of the specific enthalpy of the solid phase and gaseous phase, when only air is present:

$$h_m = \frac{\rho_s h_s (1-\phi) + \phi \rho_a h_a}{\rho_m} \tag{4.13}$$

Using equation 4.13,4.1 and 4.3, we can write

$$w_s h_s + w_a h_a = (1-\phi)\rho_s h_s + (\phi - \phi_l)\rho_a h_a = \rho_m h_m - \phi_l h_a \rho_a \tag{4.14}$$

Thus, H_{pm} becomes

$$H_{pm} = \rho_m h_m - \phi_l \rho_a h_a + w_l h_l + w_v h_v \tag{4.15}$$

and using equations 4.5,4.2 and 4.4

$$H_{pm} = \rho_m h_m - w\frac{\rho_a}{\rho_l} h_a + w h_l + (w_{cs} - w)\frac{\rho_v}{\rho_l} h_v \tag{4.16}$$

4.2.3 Total mass balance in fluid media

In additions to the assumptions needed for the derivation of the balance equations for the porous media, the following further assumptions will be done in this thesis:

1. Moist air is a mixture of two ideal gases, dry air and water vapour
2. There is no condensation in moist air. This means that there are no droplets, and only one phase, gaseous phase, can be recognized.
3. Moist air is considered to be incompressible, even if density variations can occur through the variation of concentration and temperature.
4. Momentum source are not taken into account

Assumptions 1 and 2 allow us not to take into account for a water-air interface.

If we call ρ_g the density of the total gas phase, we can write the density of water vapour and dry air, in $\left[\frac{kg}{m_g^3}\right]$, using Dalton's law of partial pressures

$$\rho_v = \frac{p_v M_v}{RT} = \frac{y_w p_g}{R_v T} \tag{4.17}$$

$$\rho_a = \frac{p_a M_a}{RT} = \frac{y_a p_g}{R_a T} \tag{4.18}$$

where p_g is the total pressure, that in this thesis is equal to 101325 Pa, M_v,M_a, y_w and y_a are the molar masses and the mole fractions of water and dry air, and R is the universal gas constant.

The total gas density can be written as

$$\rho_g = \rho_a + \rho_v = \frac{M_a p_a}{RT} + \frac{M_v p_v}{RT} = \frac{p_g}{RT}\left(M_a x_a + M_v x_v\right) = \frac{p_g M_g}{RT} \tag{4.19}$$

This means that even if the total gas pressure is considered constant, gas density can change due to a temperature or concentration variation. Anyway, in order to simplify the balance equations, we will assume the total density as constant, with the only exception of the gravitational term in the momentum equation.

The total gas flux can be written as

$$J_g = \rho_g \mathbf{v_g} = (\rho_a + \rho_v)\mathbf{v_g} = \rho_a \mathbf{v_a} + \rho_v \mathbf{v_v} = J_a + J_v \tag{4.20}$$

where $\mathbf{v_a}$ and $\mathbf{v_v}$ are the air and vapour velocity. We can consider these velocity as absolute velocity, composed by the gas velocity and a relative velocity:

$$J_a = \rho_a \mathbf{v_a} = \rho_a(\mathbf{v_g} + \mathbf{v_{r,a}}) = J_a^a + J_a^d \tag{4.21}$$

$$J_v = \rho_v \mathbf{v_v} = \rho_v(\mathbf{v_g} + \mathbf{v_{r,v}}) = J_v^a + J_v^d \tag{4.22}$$

where J_i are the convective fluxes, that can be described as the combined action of the advective fluxes J_i^a and diffusive fluxes J_i^d.

The diffusive fluxes can be written as in 2.12, since the overall gaseous density is considered constant.

The total mass balance for the humid air can be written as:

$$\frac{\partial \rho_g}{\partial t} = -\nabla \cdot (J_g) \tag{4.23}$$

Where ρ_g is the total density of the humid air.

4.2.4 Vapour balance in fluid media

The vapour balance in the fluid can be written as:

$$\frac{\partial \rho_v}{\partial t} = -\nabla \cdot (J_v) \tag{4.24}$$

Where ρ_v is the vapour density and J_v is the convective vapour flux.

4.2.5 Energy balance in fluid media

The considered mechanisms of heat transfer are enthalpy flows and conduction, thus the energy balance in the fluid can be written as:

$$\frac{\partial H_g}{\partial t} = -\nabla \cdot (q^e + q^c) \tag{4.25}$$

Where $H_g \left[\frac{kJ}{m^3}\right]$ is the total enthalpy of the fluid media; q^e and q^c are th enthalpy and the conductive heat fluxes respectively.

Conduction is predominant near the porous material walls and can be taken into account through Fourier's law:

$$q^c = -k_g \nabla T \tag{4.26}$$

where k_g is the humid air thermal conductivity thermal conductivity.

The enthalpy heat flux q^e can be modeled considering the convective mass fluxes multiplied by the specific enthalpy of air and vapour, in $\left[\frac{kJ}{kg}\right]$

$$q^e = J_g h_g = J_a h_a + J_v h_v \tag{4.27}$$

where J_a and J_v can be replaced by equations 4.21 and 4.22.

4.2.6 Momentum balance in fluid media

The velocity field of the gaseous phase can be found through the use of the Navier-Stokes equation for a Newtonian and incompressible flows:

$$\frac{\partial(\rho_g \mathbf{v_g})}{\partial t} + \nabla \cdot (\rho_g \mathbf{v_g} \otimes \mathbf{v_g}) = \nabla \cdot (-\mathbf{pI} + \mu \nabla \mathbf{v_g}) + \mathbf{g}\rho_\mathbf{g} \tag{4.28}$$

where $\otimes$ denotes the dyadic product, p is the pressure, $\mathbf{I}$ is the identity matrix and μ is the gas dynamic viscosity. With no further assumptions, equation 4.28 can be also written as

$$\rho_g \frac{\partial \mathbf{v_g}}{\partial t} + \rho_g \mathbf{v_g} \nabla \mathbf{v_g} = \nabla \cdot (-\mathbf{pI} + \mu \nabla \mathbf{v_g}) + \mathbf{g}\rho_\mathbf{g} \tag{4.29}$$

In some building physics simulations, like the computation or the total thermal resistance of a wall of hollow bricks, a natural convection flow must be considered. In this thesis, the buoyancy-driven flow is taken into account through the Boussinesq approximation. The buoyancy force is caused by a density difference in the gaseous phase, in the presence of the gravitational field. Even if the gaseous phase is considered as incompressible, we can still take into account small density changes considering the ideal gas law. Considering the total pressure p_g as constant and equal to 101325 Pa, the ρ_g depends on temperature and vapour concentration, as can be seen from 4.19. Therefore, choosing an initial reference state, we can write the gas density through a first order truncated Taylor series as

$$\rho_g = \rho_{g,0} + \left.\frac{\partial \rho_g}{\partial T}\right|_0 \Delta T + \left.\frac{\partial \rho_g}{\partial x_v}\right|_0 \Delta x_v = \rho_{g,0} + \Delta\rho_g \tag{4.30}$$

where the subscript $_0$ denotes the reference state, and the Δ operates between the actual state and the reference state. For simplifying the equations, we can notice that if velocity goes to zero, the gradient of the resulting static pressure will be equal to $\rho_{g,0}\mathbf{g}$

$$\nabla p_s = \rho_{g,0}\mathbf{g} \tag{4.31}$$

Assuming that the total pressure can be written by the sum of the static pressure and a dynamic pressure due to the velocity field,

$$p = p_s + p_d \tag{4.32}$$

thus the total pressure gradient can be written as

$$\nabla p = \nabla p_d + \rho_{g,0}\mathbf{g} \tag{4.33}$$

Replacing now 4.30 and 4.33 into 4.28, the momentum balance equation becomes

$$\frac{\partial(\rho_g \mathbf{v_g})}{\partial t} + \nabla \cdot (\rho_g \mathbf{v_g} \otimes \mathbf{v_g}) = \nabla \cdot (-p_d \mathbf{I} + \mu \nabla \mathbf{v_g}) + \mathbf{g}\Delta\rho_g \tag{4.34}$$

The change in the pressure reference, from the absolute pressure p to the dynamic pressure p_d can be ignored when pressure is not specified on boundary conditions, according to [2].

If the total pressure is considered constant, the variation in gas density are due to changes in temperature and in vapour concentration. The influence of these two variables on gas density is the following:

$$\Delta\rho_g = \left.\frac{\partial \rho_g}{\partial T}\right|_0 \Delta T + \left.\frac{\partial \rho_g}{\partial x_v}\right|_0 \Delta x_v \tag{4.35}$$

where the subscript 0 stands for the conditions in the reference state.

Considering that the gas density can be written as:

$$\rho_g = \frac{p_g M_g}{RT} = \frac{p_g \left(M_v x_v + M_a x_a\right)}{RT} = \frac{p_g \left(x_v \left(M_v - M_a\right) + M_a\right)}{RT} \tag{4.36}$$

using equation 4.36 in combination with 4.35, we can write

$$\Delta\rho_g = -\left.\frac{p_g M_g}{T^2 R}\right|_0 \Delta T + \left.\frac{\left(M_v - M_a\right) p_g}{RT}\right|_0 \Delta x_v \tag{4.37}$$

4.3 Balance equations with temperature and relative humidity as potentials

In this thesis, the balance equations are written assuming temperature and relaive humidity as potentials. While relative humidity can be replaced by capillary pressure, as already mentioned in chapter 2.2, p_c is not defined in non capillary-active materials, and there will be no physical meaning in using it. Chosing relative humidity as a potential results in a non-conservative form of the differential equation for water balance in the porous media, as showed in [11] and [27], since the derivative of φ with respect to time is multiplyed by the water storage function, which depends on φ. Anyway, with small enough time steps, the mass conservation error affecting the solution is not significant, as investigated in [26].

The following equations are derived from equations 4.9, 4.10, 4.24, 4.25 in appendix A.

Mass balance in porous media

$$\frac{\partial w}{\partial \varphi}\frac{\partial \varphi}{\partial t} = -\nabla \cdot (-D_{m\varphi p}\nabla\varphi - D_{mTp}\nabla T) \tag{4.38}$$

Energy balance in porous media

$$d_T\frac{\partial T}{\partial t} + \nabla \cdot (-D_{e\varphi p}\nabla\varphi - D_{eTp}\nabla T) = -d_\varphi\frac{\partial \varphi}{\partial t} \tag{4.39}$$

Vapour balance in fluid media

$$F\frac{\partial \varphi}{\partial t} + \nabla\cdot(-D_{m\varphi a}\nabla\varphi - D_{mTa}\nabla T) + \varphi\left(\frac{\partial F}{\partial t} + \mathbf{v}\frac{\partial F}{\partial T}\nabla T\right) + F\mathbf{v}\nabla\varphi = 0 \tag{4.40}$$

Energy balance in fluid media

$$\frac{\partial \varphi}{\partial t}F(h_v - h_a) + \frac{\partial T}{\partial t}\left[\varphi\frac{\partial F}{\partial T}(h_v - h_a) + F\varphi(c_{p,v} - c_{p,a}) + \rho_g c_{p,a}\right] =$$
$$-\mathbf{v}(A_\varphi\nabla\varphi + A_T\nabla T) - \nabla\cdot(-D_{e\varphi a}\nabla\varphi - D_{eTa}\nabla T) \tag{4.41}$$

4.3.1 Line source model equations

The line source model equations are obtained through a mass and energy balance for an infinitesimal control volume.

We'll consider the case of a indefinite channel which can exchange mass and energy from the upper face, and with a adiabatic and impermeable lower face.

We can write a generic balance for the transported quantity u, and obtain the specific transport equations.

If we call A the cross section area of the channel, S the lateral surface,and δV the infinitesimal control volume, we can write the balance of a generic quantity u, transported ny the air streaming, as:

$$\delta V\frac{\partial u}{\partial t} = A(\Gamma(x) - \Gamma(x + \delta x)) + \phi S \tag{4.42}$$

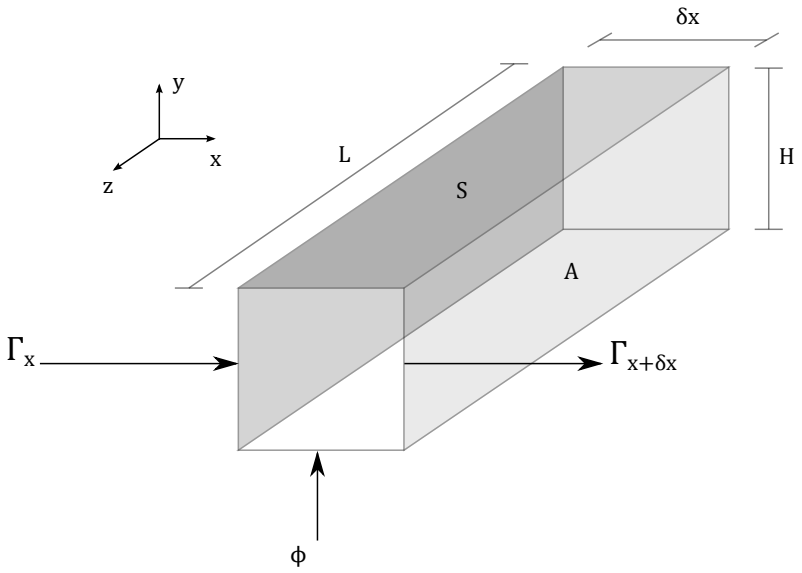

Figure 7: continuity balance on an infinitesimal volume element

If the channel was open to mass and energy flux also from the lower face, S should have been multiplied by 2.

We can write $\Gamma(x+\delta x)$ as a truncated Taylor series:

$$\Gamma(x+\delta x) = \Gamma(x) + \frac{\partial \Gamma(x)}{\partial x}\delta x \tag{4.43}$$

substituting 4.43 in 4.42 rewriting the surfaces we obtain:

$$HL\delta x\frac{\partial u}{\partial t} = -HL\frac{\partial \Gamma}{\partial x}\delta x + L\phi\delta x \tag{4.44}$$

that leads to:

$$\delta x\frac{\partial u}{\partial t} = -\frac{\partial \Gamma}{\partial x}\delta x + \frac{\phi\delta x}{H} \tag{4.45}$$

We can now write the conservation of vapour density and energy, substituting the quantity u with the vapour density ρ_v and the enthalpy h, Γ with the fluxes of water vapour and enthalpy and ϕ with the mass and energy quantities exchanged with the wall, we obtain:

$$\frac{\partial \rho_v}{\partial t} = -\mathbf{v}\frac{\partial \rho_v}{\partial x} + \frac{\beta(p_v^{wall} - p_v)}{H} \tag{4.46}$$

$$\frac{\partial h}{\partial t} = -\mathbf{v}\frac{\partial h}{\partial x} + \frac{\alpha(T^{wall} - T)}{H} + \frac{\beta(p_v^{wall} - p_v)h_v}{H} \tag{4.47}$$

where

$$h = T\rho_a c_{p,a} + h_v$$

and

$$h_v = (Tc_{p,v} + H_{ev})\rho_v$$

note that p_v represents the bulk partial pressure of the vapour and T represents be the bulk temperature.

5 Case studies

5.1 Isothermal drying

The purpose of this first simulation is to compare our model for heat and mass transfer inside a porous media with the one used by Delphin. For doing this we have chosen a particularly challenging case from the numerical point of view, as explained in 5.1.1

Delphin is a commercial numerical simulation tool for combined heat, moisture, air and salt transport in porous building materials [54]. It is mostly applied to calculate transient processes in building envelopes in order to predict the moisture risk and the durability of the construction. The software is developed using finite-voloume technique, which is considered for some aspects to be numerically inferior to finite-element technique [27]. This is due to the fact that the finite-element technique explicitly assumes a variation of the independent variables over the domain. Moreover, the values on the surfaces of the discretized elements for the variables and the fluxes have to be calculated if the finite-volume technique is used, leading to additional approximations (see appendix C.1). Anyway, has been shown that for the heat and moisture transfer, the finite volume approach seems to provide more stable solutions [45].

Delphin is limited to two-dimensional cases. Moreover, Delphin does not allow fluid dynamics modeling inside air gaps between the building components. Convection is taken into account applying third-type boundary conditions with constant transfer coefficients.

Delphin was testing according to HAMSTAD Benchmarks 1 to 5, EN 15026:2007. The software was also validated to conform with both two-dimensional cases of ISO 10211:2007, Annex A.

5.1.1 Simulation setup

As a test case we consider the drying process of a moist porous material (brick) as described in [26].

The simulation is mono dimensional for the sake of simplicity.

The material is dried from the right side, which is open to mass and energy transfer, while the left side is open to energy transfer but considered close for mass transfer (see figure 8). The fluid conditions outside the boundary layer are constant in time.

The boundary conditions are described by equations 5.1,5.2,5.3,5.4:

$$q(0,t) = -\alpha(T(0,t) - T_\infty) \tag{5.1}$$

$$J_v(0,t) = 0 \tag{5.2}$$

$$q(l,t) = -\alpha(T(l,t) - T_\infty) + J_v(l,t)(H_{ev} + c_{p,v}T) \tag{5.3}$$

$$J_v(l,t) = -\beta(p_v(l,t) - p_{v,\infty}) \tag{5.4}$$

where q is the heat flux and J_v represents the vapour flux; α and β are the convective heat and mass transfer coefficients respectively. H_{ev} is the enthalpy of vaporization and $c_{p,v}$ is the thermal capacity at constant pressure of the water vapour. Using temperature and relative humidity as potentials, the partial pressure of water vapour is defined by equation 5.5

$$p_v = \varphi p_s(T) \tag{5.5}$$

The initial conditions and the air conditions outside the boundary layer are shown in figure 8.

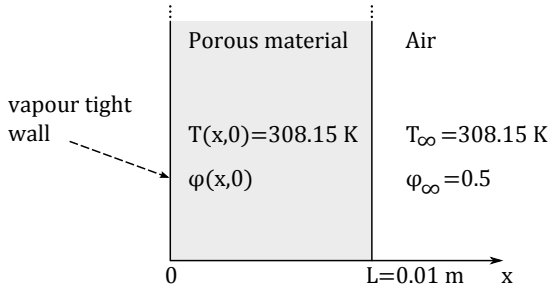

Figure 8: Schematic representation of the 1D test problem.

In this study two cases are considered.

In the fist case the initial relative humidity is considered to be 0.9999, as previously done in [26].

In that study the author employ an initial relative humidity slightly under the unity, since a complete saturation leads to higher numerical difficulties. At 100% relative humidity small oscillations can occur during calculations, even if a implicit temporal method is used and even with a high absolute tolerance. In the second case the initial relative humidity is equal to 1. In order to avoid errors due to the water storage function derivative, the procedure described in appendix C.3 is used.

At the beginning of this experiment, the brick and the bordering air are isotherm (see figure 8). The temperature inside the brick changes only due to convective drying. This case is particularly interesting since equation terms which are in general negligible, have to be taken in account in order to see the drop in temperature. Those terms are:

1. energy transport due to evaporation at the surface

$$J_v(H_{ev} + c_{p,v}T) \tag{5.6}$$

2. energy transport due to capillary liquid conductivity

$$-K_l \frac{\partial p_c}{\partial \varphi} c_{p,l} T \tag{5.7}$$

The energy transport due to evaporation is considered in equation 5.3. The capillary transport is significant only above 0.5 relative humidity [31] and is taken into account through an experimental function as is done for the water storage function (see equation A.4). The total enthalpy is considered by equation A.20.

This particular set up is particularly challenging from a numerical point of view for two reasons:

1. *Steep gradients* of the system variables. During the simulations, very steep gradient of temperature and relative humidity are present, as explained in chapter 5.1.3. These steep gradients can lead to numerical difficulties.

2. *Saturation condition inside the material.* The transport equations A.9 and A.21 are highly non linear. This non linearity is mainly due to the shape of the water storage function (see figure 3) . When the relative humidity approaches unity, the derivative of the water storage function becomes very high. For this reason under saturation conditions, numerical errors are amplified.

5.1.2 Numerical setup

In COMSOL the default time-dependent solver for the pde equations is the IDA solver, which uses variable-order varible-step-size backward differentiation formulas (BDF).

The order of the BDF can vary from one (that is backward Euler) to 5. There is also a second solver called the Generalized-α solver, which has properties similar to the second-order BDF solver. Through the parameter α it is possible to control the degree of damping of high frequencies. Compared to BDF (with maximum order two), Generalized-α causes much less damping and is thereby more accurate, but it is also less stable.

For this simulation we have chosen the BDF solver, with a variable order from 1 to 5 in order to better predict the steep gradient that appears near the 40th hour (for the simulation which starts at saturation).

The time step is also kept variable in order to increase the accuracy during the transition zone, without increasing too much the computational time. This can be done, since COMSOL automatically chooses the time step through a constraint on the relative and absolute tolerance.

More specifically, the absolute and relative tolerance control the error with the following formula:

$$\left(\frac{1}{M_f} \sum_j \frac{1}{N_j} \sum_i \left(\frac{|E_i U_i|}{A_{u,i} + R_t |U_i|} \right)^2 \right)^{\frac{1}{2}} < 1 \tag{5.8}$$

whereM_f is the number of fields, N_j is the number of degree of freedom in the field j. U is the solution vector corresponding to the solution at a certain time step and E is the solver estimate of the local error during the time step. $A_{u,i}$ is the unscaled absolute tolerance for the degree of freedom i, R_t is the relative tolerance.

In general, it is advantageous to choose a different value of the absolute tolerance for different system variables. For example, for this specific case, the absolute error for temperature should be different from the absolute error for relative humidity, since temperature is typically in the order of 10^2K, while relative humidity is always under unity.

In order to have more control on the constraint, we have chosen a very low absolute error for all the variables (in the order of 10^{-10}). This makes the relative tolerance the ruling criterion for the error control, according to equation 5.8. The relative tolerance has been set to the value of 10^{-5}, since it is the same used by the Delphin solver.

5.1.3 Results

Error and uncertainty are unavoidable in numerical simulations. It is therefore necessary to develop a rigorous method to quantify the quality of the results. Two main aspects are widely recognized in order to provide trustable results:

1. Verification: this is the process of determining if the solution of the simulation accurately represents the model written by the developers. This process quantify the errors that occurs in the process of discretizing and solving the mathematical model.

2. Validation: this is the process of investigating the accuracy of the model in predicting the experimental data. This process quantify the uncertainties.

The validation process in this study is obtained through comparison of the results with Delphin software, which has been validated itself with experimental results [1]. The verification process is considered in chapter 5.1.4.

The accuracy of the solution is investigated using three grid levels, which are refined sequentially by slicing the spatial step in half. The first level uses 50 elements, the second one 100 and the third 200.

In figure 9 and 10 are plotted the results of COMSOL and Delphin. The figure shows the temporal development of temperature and relative humidity calculated at the right boundary. Only the results with 50 and 100 elements have been plotted, since the last mesh did not show significant improvement in the accuracy of the solution in both COMSOL and Delphin. In the case of Delphin, the differences are negligible even between the results obtained with a 100 elements and a 50 elements mesh. In this case Delphin seems to be more stable on coarser meshes.

The simulation studies the transition between the two main phases of a drying process. During the first phase, also called the constant dry rate period, the water transport is mainly due to capillary conductivity. The water transported

from the inside of the domain to the right boundary evaporates at the external surface so that the temperature decreases due to evaporation cooling (see figure 9 and 10). In this first phase the relative humidity maintains his value close to 1. In the second phase, known as the decreasing dry rate period, a steep gradient of relative humidity appears at the surface of the porous material. This leads to a rise of surface temperature, since the cooling effect of evaporation is drastically reduced. For these reasons we have a very steep gradients of relative humidity and temperature during the simulation.

From the results we can see the influence of the initial values of the relative humidity. In the case in which initial relative humidity has been chosen equal to 0.9999, the transition between the two main phases of the drying process appears during the 11th hour. In the case with 100% initial relative humidity the transition appears during the 40th hour, so we can see how a very small difference in the initial condition of relative humidity, can bring to relative differences of 250% in the time of appearance of the drying front. This is due to the shape of the water retention curve (see figure 3): at relative humidity near unity the curve increase steeply, leading to a very high water storage capacity in the porous material.

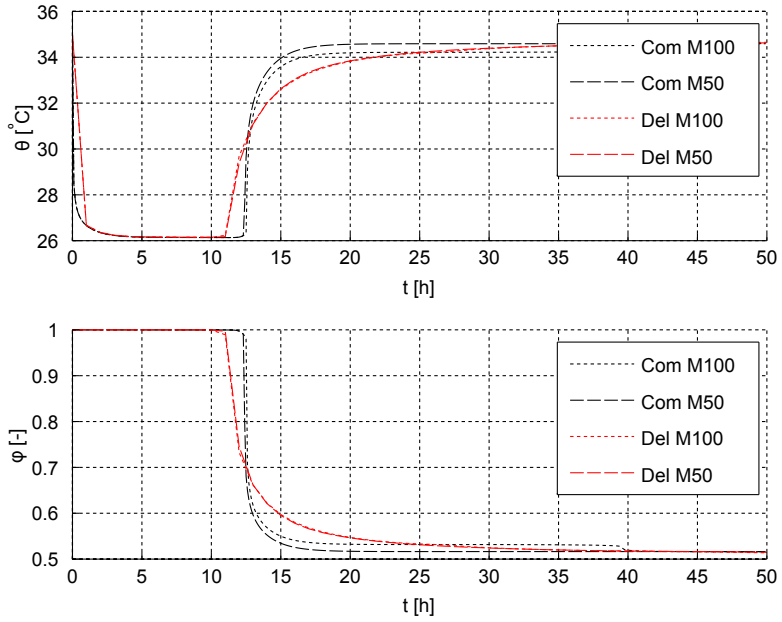

Figure 9: Temporal development of temperature and relative humidity calculated at the right boundary, with different number of elements and with $\varphi(x, 0) = 0.9999$. Comparison of Delphin and COMSOL simulations. There is no significant deviation between the Delphin solutions for the mesh with 50 and 100 elements.

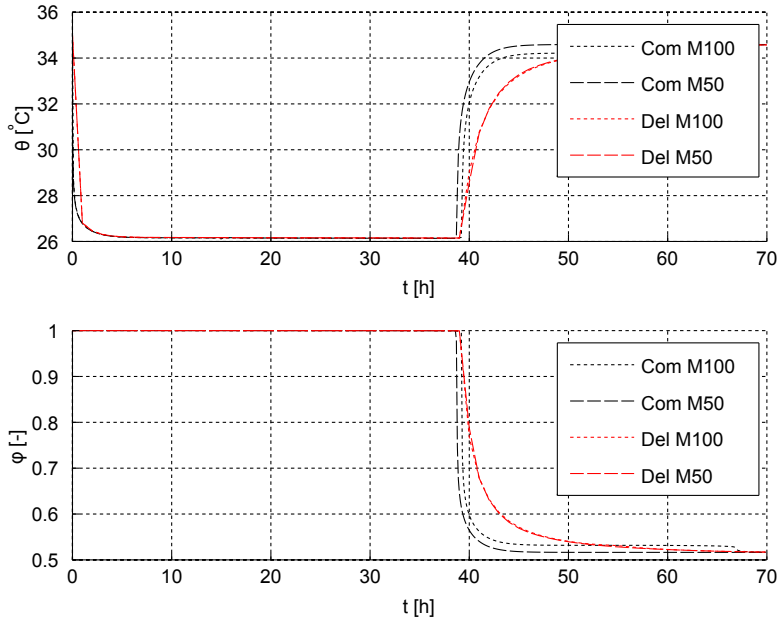

Figure 10: Temporal development of temperature and relative humidity calculated at the right boundary, with different number of elements and with $\varphi(x, 0) = 1$. Comparison of Delphin and COMSOL simulations. There is no significant deviation between the Delphin solutions for the mesh with 50 and 100 elements.

Comparing the results of COMSOL with those obtained with Delphin, we observe that both softwares capture correctly the main evolution of the drying process. However, the COMSOL solution presents non physical oscillations. These irregularities can be reduced using cubic shape functions instead of linear, as was further investigated in [26], or increasing the number of elements near the right boundary.

5.1.4 Numerical quality of the solution

Various errors can be investigated in the verification process. Amongst them there are computer coding errors and users errors, which we are not able to quantify. Round off errors can be assessed by comparing results obtained using different levels of machine accuracy, which is not possible in general for commercial codes. One of the main errors in numerical computation are due to discretization errors. Those are due to the fact that the solution can be obtained only in a finite number of points in space and time.The easiest way to investigate discretization errors is to obtain a series of solutions of the same problem with progressively refined meshes. In this way it is possible, under

certain conditions, to approximately calculate the discretization error.

According to [39, 18] this is possible if the solution satisfies the following conditions:

- The solution is smooth enough to justify the use of Taylor series expansions.This means that any discontinuity should be avoided.
- The convergence is monotonic, which means that if the quantity of interest reduces upon going from a coarse mesh to a finer mesh, its value should again reduces if the mesh is refined again.

If we denote with u the exact solution of the mathematical equations, the estimates of the discretization errors are in the form

$$||u - u_h|| \leq Ch^P \tag{5.9}$$

where u_h is the solution obtained with a mesh with elements of size h, P is the order of convergence as the mesh spacing h decreases and C is a constant.

The norm used in 5.9 is the L^2 norm, that is an appropriate norm for investigating finite element method errors, according to [17, 18, 61, 10], and is defined as:

$$||u|| = \left(\int u^2 \, \mathrm{d}\mathbf{x} \right)^{\frac{1}{2}} \tag{5.10}$$

It is common practice to use a reference solution as exact solution if the last is not known for the problem that is being investigated. We have obtained the reference solution on a grid of 400 elements, with an absolute and relative tolerance of 10^{-12}. This method can be used as well in transient problems to obtain an approximation of the discretization error due to finite time step size. Since COMSOL automatically changes the time step in order to satisfy the convergence constrain of the absolute and relative tolerance, we only investigate spatial discretization errors, as done in [60]. The procedure described in [61] for computing the L^2 norm has been applied.

The assessment of the convergence error is performed considering that the error of the first mesh is given by equation 5.11

$$||u - u_h|| \leq Ch^P \tag{5.11}$$

The error of the next finer mesh with mesh spacing $\frac{h}{2}$ is

$$||u - u_{\frac{h}{2}}|| \leq C(\frac{h}{2})^P \tag{5.12}$$

and their ratio is

$$\frac{||u - u_h||}{||u - u_{\frac{h}{2}}||} \leq \frac{Ch^P}{C(\frac{h}{2})^P} \tag{5.13}$$

.

For a refinement that halves the size of the mesh elements, an estimation of the convergence error can be therefore written as

$$P = log_2 \left(\frac{||u - u_h||}{||u - u_{\frac{h}{2}}||} \right) = log_2 \left(\frac{E_1}{E_2} \right) = ln \left(\frac{E_1}{E_2} - 2 \right) \tag{5.14}$$

where E_1 is the norm of the difference between the correct solution and the solution of the coarse grid and E_2 is the norm of the difference between the correct solution and the solution of the finer grid.

Since the smoothness of the solution is required, the boundary conditions for humidity of the air outside the boundary layer (see figure 8) are modified. Initially the relative humidity of the surrounding air is taken equal to the relative humidity inside the porous material (0.9999). The condition is then changed applying a smooth ramp to this value that brings the boundary condition for air humidity to the value of 0.5, as in the previous study. The ramp is chosen to have continuous second derivative and with a transition zone of 10% of the total simulation time.

For the convergence study four grids have been considered, with uniform element size and linear Lagrange elements. The absolute tolerance has been set to 10^{-10} and the relative tolerance to 10^{-7}. The order of convergence has been estimated on both the values of temperature and relative humidity. In table 3 the relative normalized error and the assessment for the convergence error is reported. The relative normalized error has been calculated as:

$$R_h = \frac{||u - u_h||}{||u||} \tag{5.15}$$

where u is the reference solution. All the values of table 3 are mean values in time.

Table 3: Relative normalized errors and assessment of the convergence index for various discretizations. Time mediated values.

Grid	Elements	$R_h(\varphi)$	$R_h(T)$	p (φ)	p (T)
1	25	6.05e-2	7.1e-3		
2	50	2.47e-2	3.5e-3	1.04	1.011
3	100	1.47e-2	1.74e-3	1.004	1.047
4	200	6.61e-3	7.7e-4	1.14	1.175
5	400				

notice that, as expected, the relative normalized errors decrease as the element size decrease. For Lagrange elements with linear shape functions, the theory predicts $P = 2$, that is, quadratic convergence of the norm of the solution error. However, especially in case of complex equations, this is not always true, as investigated in [10].

This study reveals that the convergence order for this problem seems to be linear, that is, we can expect a linear decrease of the error with the size of the mesh.

5.2 Comparison of the conjugate model and line source model with experimental data

In this chapter the numerical solution from the conjugate and from the line source approach are compared with the experimental and the benchmark data from [24].

The benchmark data is provided by eight different models that have been developed by the following universities:

- Katholieke Universiteit Leuven, Belgium [27]
- Slovak Academy of Science, Slovakia [32]
- Concordia University, Canada [59]
- IRC-NRC, Canada [58]
- Technical University of Dresden, Germany [49]
- Chalmers University of Technology, Sweden [28]
- Thermal Science Centre of Lyon, France [35]
- University of Saskatchewan, Canada [46]

In this study, an element composed by three overlapped gypsum boards, is firstly humidify and than dried by a fully developed laminar flow (see image 11) . The inlet conditions of the flow and initial conditions for temperature and relative humidity are listed in table 4.

Table 4: Initial conditions and inflow conditions for temperature and relative humidity.

t		0	24h	48h
θ	$[^oC]$	23.3	23.8	22.5
φ	$[-]$	0.3	0.719	0.296

Must be pointed out that all conditions in table 4 are an approximation of the real conditions. In particular, the initial values for relative humidity is known to be between 0.3 and 0.35, and the values of temperature and relative humidity for the inlet flow are assumed constant even if the measured values are time dependent (see [24] for further details). In order to compare the conjugate model with the results from the other eight models , the constant values of Table 4 are employed, as done by the other authors. All the material properties, as well

as the moisture storage function, were provided by the author in [24]. Capillary conduction has not been taken into account, since the author did not provide a capillary conduction curve. Moreover, water transport due to capillary suction should be negligible compared to water transport due to vapour diffusion, since the value of relative humidity does not exceed 75% for all the simulation time in all the domain.

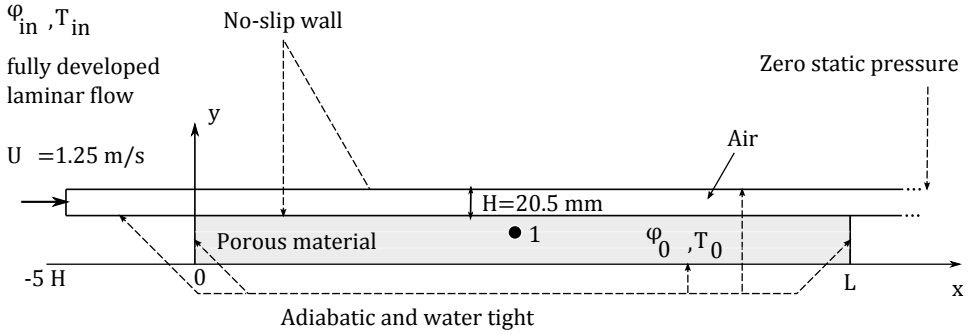

Figure 11: Geometry and boundary conditions for the study

In figure 12, the temporal development of relative humidity and temperature from the conjugate model and line-source model are compared with the experimental data and with the results from the other models. The values refers to a depth of 12.5 mm, and with $x = \frac{L}{2}$ (point 1 in figure 11); anyway, the problem can be considered mono-dimensional, so relative humidity and temperature at a certain depth does not show a significant variation along the x coordinate. The dashed lines represent the maximal and minimal solution from the other authors. For all the models, for both temperature and relative humidity, the curve of the experimental data is steeper than the one obtained with the simulations. For example, at the beginning of the simulation, derivatives in respect to time of relative humidity and temperature are lower than the one of the experimental data. A similar response can be seen after 24 hours, when the values of the boundary conditions changes. Minor deviations concerning the relative humidity are present between the various numerical results. Also the deviation in the temperature development is acceptable, considering that the absolute variation of temperature is rather small. The differences between the line source model and the conjugate model are small in this case, since we are considering a fully developed flow in forced convection.

In figure 13 the measured temperature and relative humidity values for the inlet flow have been taken as inputs, instead of the average temporal values. The differences in relative humidity values are not significant while are those concerning temperature values. This is mainly due to the fact that the variance of the measured inlet temperature values is bigger than the variance of measured inlet relative humidity values.

For both the variables, taking the inlet data as time dependent, results in a

more similar shape of the temporal simulated values curve with respect to the experimental data.

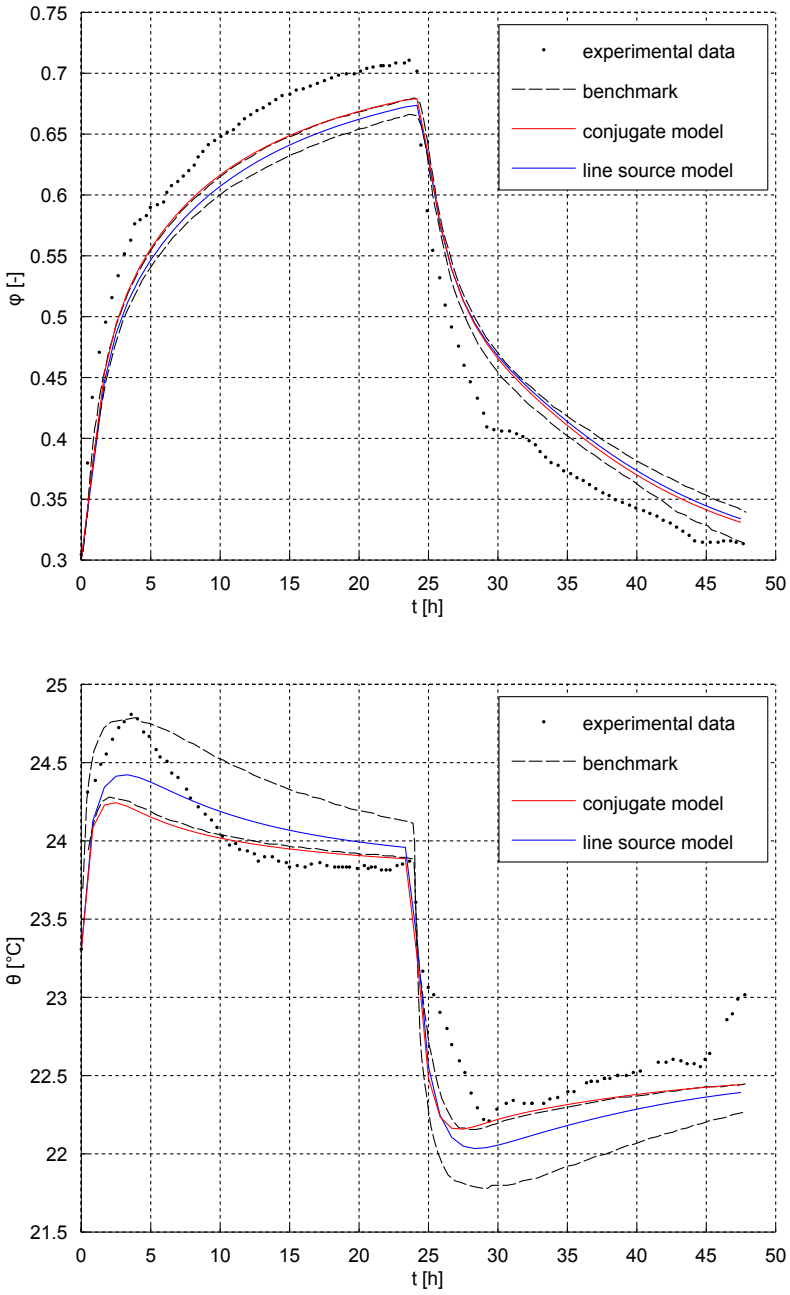

Figure 12: Temporal development of relative humidity and temperature calculated at the point 1 in figure 11. Comparison of conjugate approach and line-source approach with experimental data and benchmark solutions.

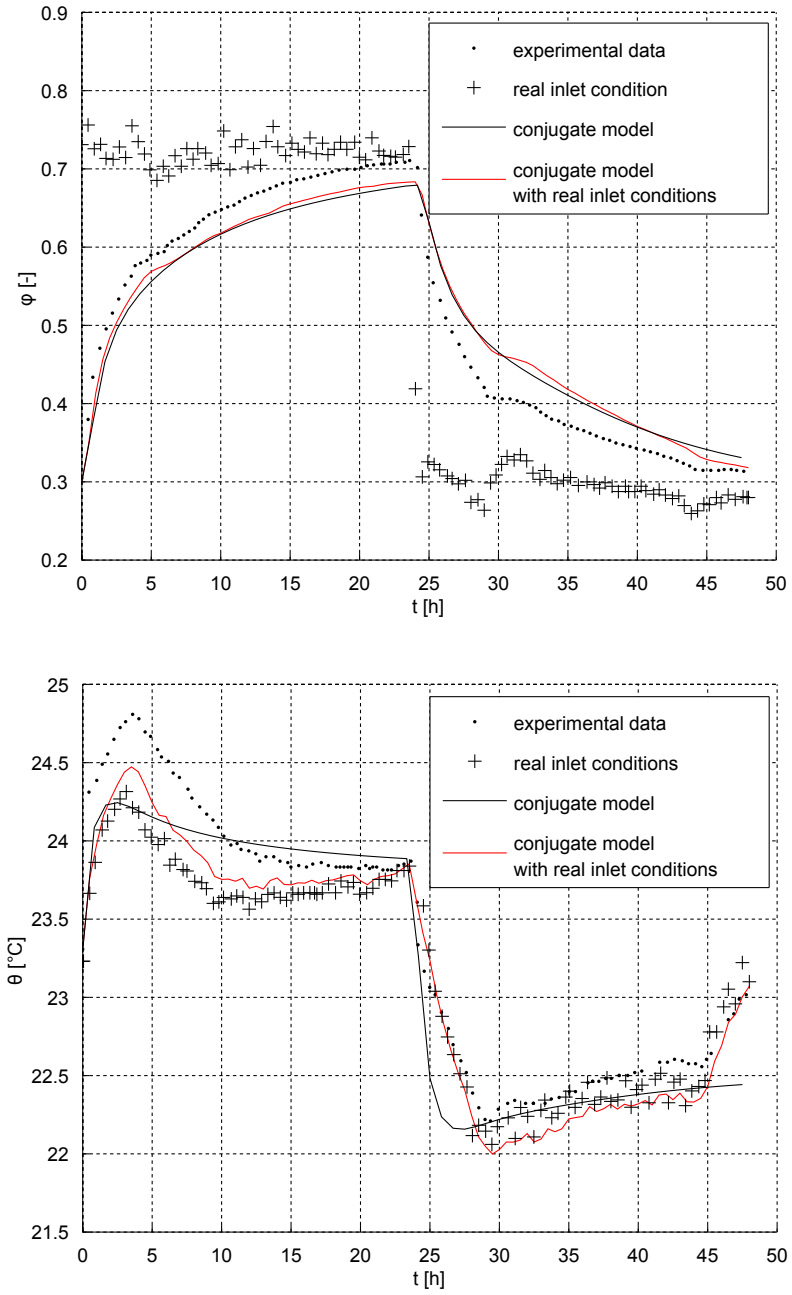

Figure 13: Temporal development of relative humidity and temperature calculated at the point 1 in figure 11. Comparison of conjugate model with constant and time dependent inlet flow boundary conditions.

5.3 Comparison of the conjugate model with the line source approach

The line source approach is a way to couple the transfer mechanism which occurs inside a porous domain with those that occurs in a free fluid flow. The fluid flow occurs inside a thin channel and is considered to be mono dimensional. His effects on the porous domain are taken into account through convective transfer coefficients, that are taken as inputs of the model. This approach cannot compute the temperature and humidity distribution inside the fluid phase, but only the bulk quantities along the channel axis (equation 5.32).

As previously said in chapter 1, a particularly important case for moisture risk analysis, is the one of wooden beam ends, since if condensation is present, it can leads to a structural damage to the wood. Including fluid dynamics in long period hygrotermal simulation increase numerical effort and computational time. Even in the case of laminar non-turbulent forced flow, the differences in term of computational time are significant. Thus, it is meaningful to investigate the differences between the solutions obtained with the conjugate model and a simplified model.

In this section, three different cases are considered. In all the cases the porous material is gypsum, and the boundary conditions for the fluid in the line source model can be summarized as follows:

$$T(x_{in}, y, t) = T_{in} \tag{5.16}$$

$$\rho_v(x_{in}, y, t) = \frac{\varphi_{in} Ps(T_{in})}{R_v T_{in}} \tag{5.17}$$

for the inflow boundary conditions, where the subscript *in* stands for inlet, and:

$$\nabla T(x_{out}, y, t) = 0 \tag{5.18}$$

$$\nabla \rho_v(x_{out}, y, t) = 0 \tag{5.19}$$

for the outflow boundary conditions, where the subscript *out* stands for outlet. This condition imposes a fully developed flow outlet condition, in therms of T and ρ_v distributions.

For the case A and B the upper part of the channel is considered to be adiabatic (see figure 14).

The porous material in case A and B is considered to be closed to the heat and mass transfer with the only exception of the upper boundary, for which the following boundary conditions apply in the line source approach:

$$J(x, t) = -\beta(p_v - p_{v,bulk}) \tag{5.20}$$

$$q(x, t) = -\alpha(T - T_{bulk}) + J(x, t)h_v \tag{5.21}$$

where α and β are the convective transfer coefficients for the heat and the mass respectively, and the subscript *bulk* stands for the bulk quantity. For the 3 cases, α and β are assumed constant and respectively equal to 46.2 $\left[\frac{W}{m^2K}\right]$ and 3e-8 $\left[\frac{s}{m}\right]$.

For the conjugate model we can use equations 5.16, 5.17, 5.18, 5.19 ,with the difference that we can use the value of φ directly in equation 5.17 and 5.19, since the equations of the conjugate model uses φ instead of ρ_v as variable.

Boundary conditions for the air flow field are of fully developed velocity profile at the inlet and zero static pressure at the outlet. A no-slip wall condition is imposed for the upper and lower boundaries, that is:

$$\mathbf{v}^{int} = 0 \tag{5.22}$$

where *int* stands for interface.

The velocity field in this simulation is considered to be stationary, since the momentum and continuity equations of the air are not dependent from the temperature and relative humidity distributions.

For the temperature and humidity fields, only continuity conditions are needed at the interface, since the heat and mass transfer are automatically computed without the need of a convective transfer coefficient. This imply that the total heat and mass flux, as well as temperature and relative humidity, have to be continuous at the interface between the porous material and the fluid.

$$J_{pm}^{int} = J_{fm}^{int} \tag{5.23}$$

$$q_{pm}^{int} = q_{fm}^{int} \tag{5.24}$$

$$T_{pm}^{int} = T_{fm}^{int} \tag{5.25}$$

$$\varphi_{pm}^{int} = \varphi_{fm}^{int} \tag{5.26}$$

where the subscript pm stands for porous media and fm for fluid media. From equations A.9, A.27, A.21, A.42 we have:

$$J_p^{int} = -D_{m\varphi p}\nabla\varphi - D_{mTp}\nabla T \tag{5.27}$$

$$J_f^{int} = -D_{m\varphi a}\nabla\varphi - D_{mTa}\nabla T \tag{5.28}$$

$$Q_p^{int} = -D_{e\varphi p}\nabla\varphi - D_{eTp}\nabla T \tag{5.29}$$

$$Q_f^{int} = -D_{e\varphi a}\nabla\varphi - D_{eTa}\nabla T \tag{5.30}$$

In a typical approach the heat and humidity transfer at the boundary is taken into account through a third type boundary condition of the type:

$$\gamma = -h_u(u_b - u_\infty) \tag{5.31}$$

where γ is the inward flux of the quantity u, and h_u, u_b e u_∞ are the convective transfer coefficient, the boundary value of u and the value of u outside the boundary layer respectively.

Considering a thin channel, we can not identify a value for u_∞, since the thickness of the channel is inferior to the boundary layer thickness. Supposing to work in a two-dimensional problem, instead of u_∞, it is therefore necessary to apply the boundary condition using the bulk quantity in the channel, u_{bulk}, which is defined as follows :

$$u_{bulk} = \frac{\int_0^L J(y)\,\mathrm{d}y}{\int_0^L f(y)\,\mathrm{d}y} \tag{5.32}$$

The line source approach balance equations are derived in appendix 4.3.1

5.3.1 Simulation setup

In this section a two-dimensional fully developed laminar channel flow is considered. Forced convection and incompressible fluid are assumed.

In the first two cases, a straight channel along the x direction is modeled (see figure 14). The upper part of the channel is insulated to the heat and moisture transfer. In the third case a different geometry is considered, with a channel between two porous domains. In this last case the channel vary his direction, so that influences of vortexes can be investigated (see figure 22) .

For the first two cases temperature and relative humidity of the air at the channel inlet and initial conditions in the fluid and porous domains, are summarized in table 5

Table 5: Initial values (left) and air inlet values (right) of temperature and relative humidity for the cases A and B.

case	φ_0 [-]	T_0 [°C]	φ_{in} [-]	T_{in} [°C]
A	0.5	10	0.7	22
B	0.7	22	0.5	10

The equations for the fluid phase in the line source model are expressed with respect to vapour density only to keep the original formulation of the balance (see appendix 4.3.1); we can still keep the variable φ for the balance in the porous media since the equations are virtually uncoupled thanks to the convective transport coefficients.

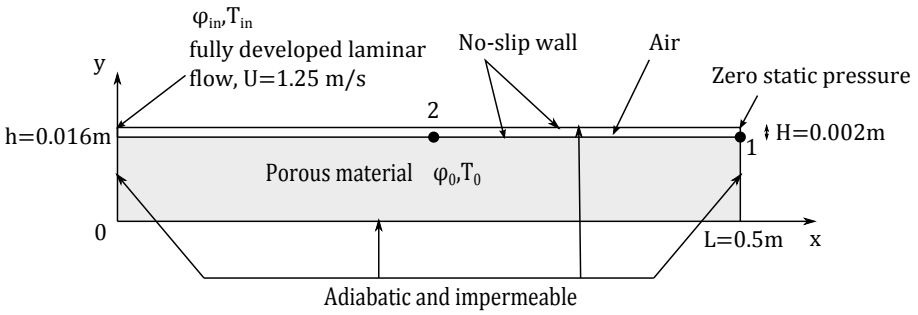

Figure 14: Geometry and boundary conditions for case A and B.

5.3.2 Study of the convergence order

The study of the order of convergence has been carried out for the porous material with four different meshes in winch the elements have been gradually refined. For the refinement, every element has been divided in both x and y directions. All the elements have the same size. The relative tolerance for this preliminary test was 10^{-5} for all the variables and 10^{-10} for the absolute tolerance. For the reference solution (grid 5) the relative tolerance was 10^{-6}.

For this case the order of convergence has been investigated. Notice that for dimension higher than one the convergence error estimates can be written as:

$$P = \frac{ln\left(\frac{R_h}{R_{\frac{h}{2}}}\right)}{ln(r)} \tag{5.33}$$

where the parameter r is defined as follows:

$$r = \left(\frac{DOF_2}{DOF_1}\right)^{\frac{1}{D}} \tag{5.34}$$

where DOF_1 are the degrees of freedom of the coarse mesh, DOF_2 are the degrees of freedom of the finer mesh and D is the number of dimensions of the problem.

The number of elements, degree of freedom and the relative normalized error of the grids are shown in table 6.

Table 6: Number of elements, degree of freedom, parameter r, convergence order assessment and relative normalized errors for relative humidity and temperature for different grids. Time mediated values.

Grid	Elements	DOF	r	$R_h(\varphi)$	$R_h(T)$	p (φ)	p (T)
1	200	492		2.54e-1	3.71e-2		
2	800	1782	1.903	1.19e-1	1.83e-2	1.23	1.07
3	3200	6762	1.947	6.03e-2	9.24e-3	1.03	1.02
4	12800	26322	1.972	2.98e-2	4.72e-3	1.01	0.97
5	51200	103842					

Even in this case we can conclude that the problem presents a linear convergence with the element size.

5.3.3 Results

Cases A and B The simulation has been computed with a relative tolerance of 10^{-5} and an absolute tolerance of 10^{-10} for both humidity and temperature. The stationary solution for the boundary field was calculated with a relative tolerance of 10^{-10} for all the variables. The shape functions are Lagrange linear. As stated in chapter 5.3.1, fully developed flow is assumed in the air gap . This is necessary, since the reference convective heat and mass transfer coefficients used for the line source equations refers to a fully developed flow, and would be incorrect in presence of a non-full developed velocity boundary layer.

The temporal development of the values of relative humidity and temperature at the interface have been plotted in the graphs of figure15 and 16, at point 1 and 2 in figure 14. The relative differences of the solutions after one and after eight hour are shown in figure 20.

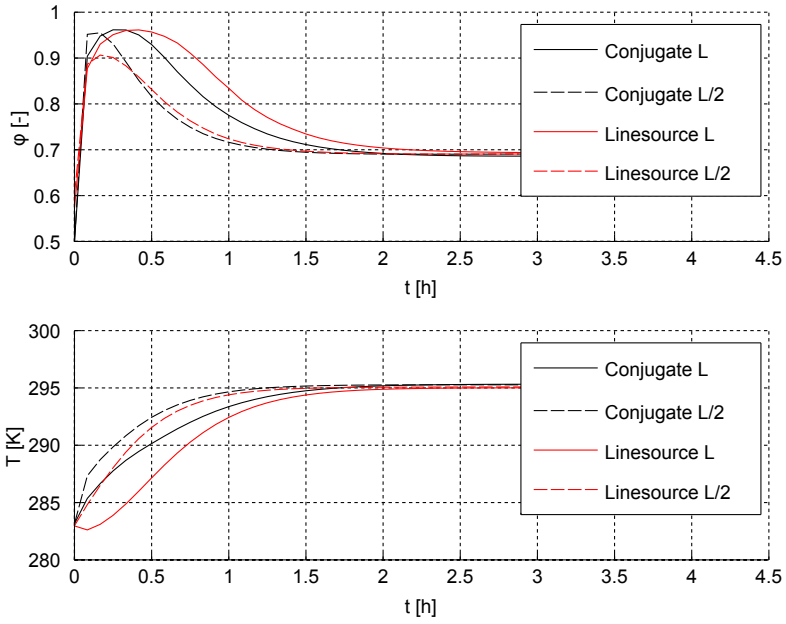

Figure 15: Temporal development of temperature and relative humidity calculated at at point 1 and 2 in figure 14. Comparison of line source approach and conjugate approach. Case A.

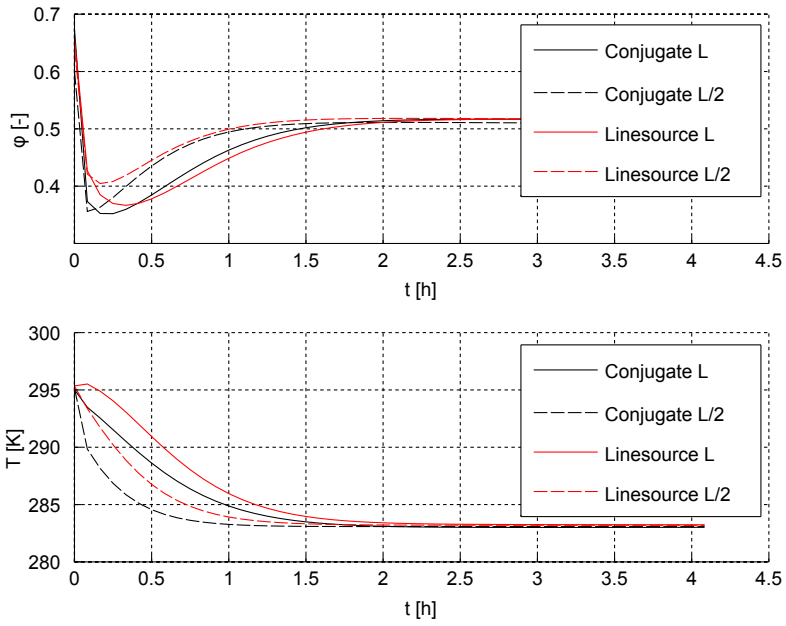

Figure 16: Temporal development of temperature and relative humidity calculated at at point 1 and 2 in figure 14. Comparison of line source approach and conjugate approach. Case B.

For better explaining the physical behavior of temperature and relative humidity in case A and B, the following considerations must be taken into account:

- *Relative velocity of mass and heat transfer in porous media:* the propagation of temperature differences are in general more rapid than a propagation in relative humidity differences inside the porous material. This can be explained considering the coefficients in equation $A.9$ and $A.21$: the typical orders of magnitude of $D_{m\varphi p}$ and D_{mTp} are 10^{-9} and 10^{-11} respectively, while the typical order of magnitude of $D_{e\varphi p}$ and D_{eTp} are 10^{-3} and 10^{1} respectively. A similar analysis can be carried out also for the diffusive transport of temperature and mass in the air; typical order of magnitude of the coefficient in equations A.27 and A.42 are: for $D_{m\varphi a}$ and D_{mTa}, 10^{-7} and 10^{-8}, for $D_{e\varphi a}$ and D_{eTa}, 10^{0} and 10^{1}.

- *Changes in relative humidity does not imply changes in water content:* relative humidity is defined as $\varphi = \frac{P_v}{P_s}$; we can use this definition to write the water vapour density, considered as an ideal gas, as

$$\rho_v = \frac{P_s \varphi}{R_v T} \tag{5.35}$$

where R_v is the gas constant for water vapour and P_s is the saturation pressure for water. The dependence of P_s from temperature is exponential (see equation A.8). This means that if temperature increases, we have an increase in vapour density, since the function $\frac{P_s}{T}$ is still an exponential. In the air, water content is only influenced by vapour density, so it is clear that increasing of relative humidity does not imply that also water content increases. In the porous media the water content includes both water vapour and liquid water, condensed inside the pores under the action of capillary pressure.

In case A, the air at the inlet is warmer and presents a higher relative humidity than the porous material. At the beginning of the simulation, since the air channel has limited thermal inertia, it decreases its temperature rapidly. For the reasons explained before, temperature variation in the air is faster than the variation of the vapour density, as can be seen in figure 17. Considering vapour density as written in equation 5.35 , and considering this value approximately constant along the x coordinate inside the channel, we can see that the change in relative humidity in the air is mainly due to the change in temperature. This cause a steep increment of the relative humidity at the interface, as shown in figure 15. After this first phase, the heat transfer from the air to the porous material causes the temperature inside the porous material to increase. In this way, the temperature of air along the channel gradually increases. If we consider again the vapour density as approximately constant inside the channel, equation 5.35 explains the decrease in relative humidity inside the porous material during the first hour (see figure 15). As the solution reaches stationary conditions, the surface temperature of the specimen reaches the air temperature values at the inlet and the value of the relative humidity inside the air decreases to the air inlet values.

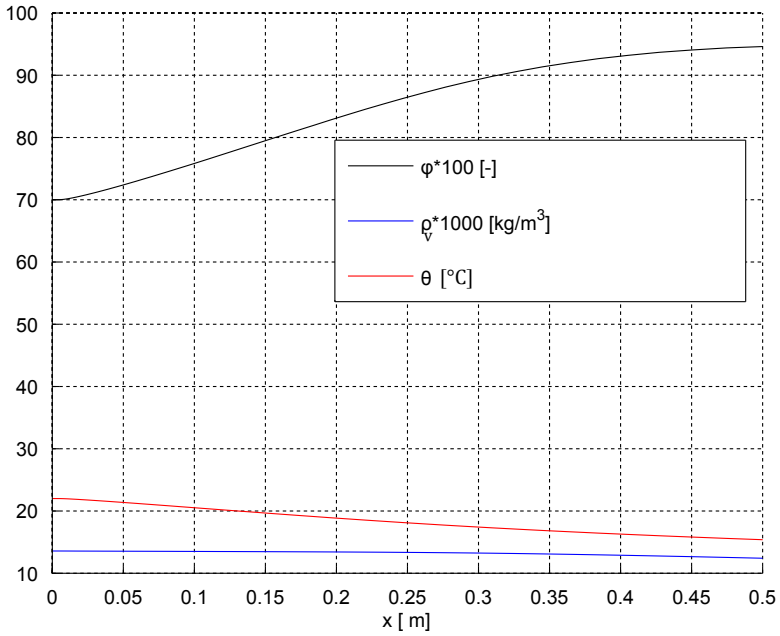

Figure 17: Values of temperature, water vapour density and relative humidity along the x coordinate taken in the middle of the air channel, at t=5s.

Similar considerations can be done in order to explain the behavior of temperature and relative humidity in case B.

The temperature and relative humidity distributions after 1 and 4 hours are shown in figure 18 for case A and in figure 19 for case B.

The relative difference between the two models is shown in figure 20 and 21 at different times. This relative difference has been calculated as

$$\frac{u_{con} - u_{line}}{u_{con}} \tag{5.36}$$

where u_{con} is the solution from the conjugate approach and u_{line} is the solution from the line source approach.

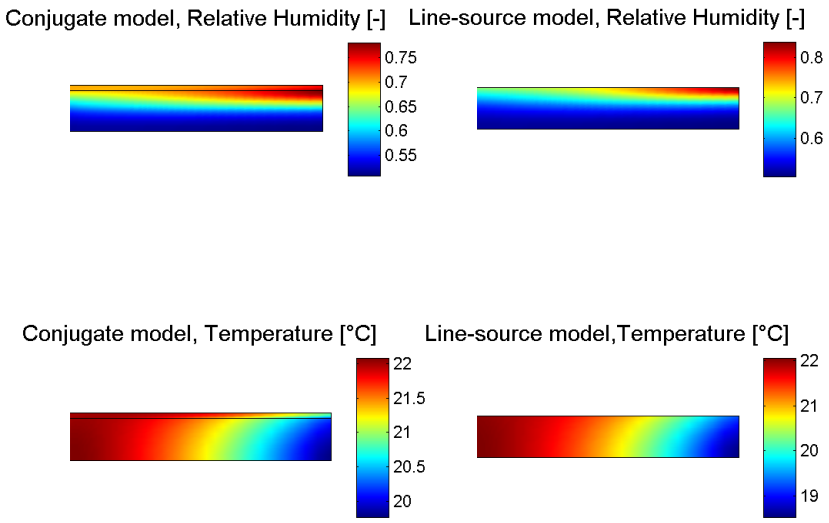

Figure 18: Relative humidity and temperature distributions for case A, after 1 h

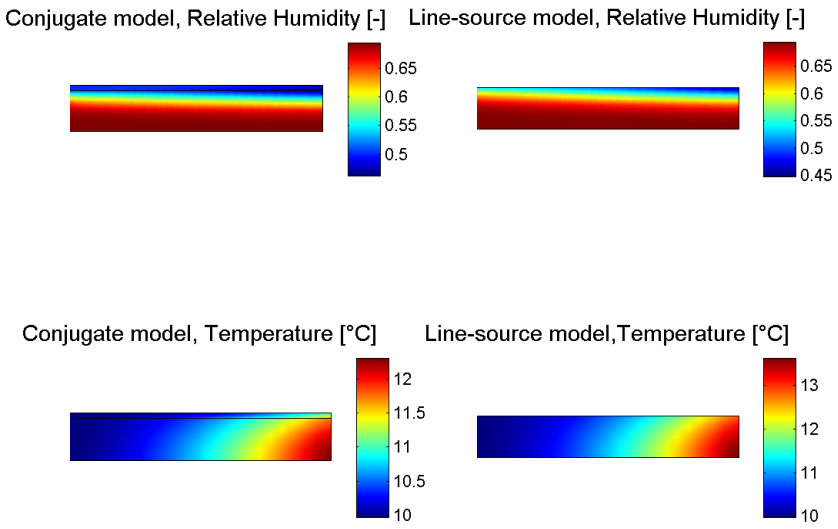

Figure 19: Relative humidity and temperature distributions for case B, after 1 h

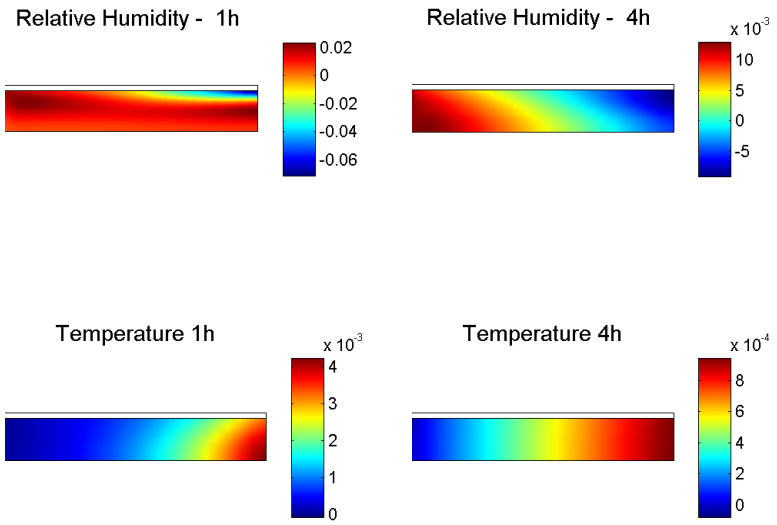

Figure 20: Relative differences between the conjugate and the line source approach, for temperature and relative humidity after 1 and 4 hours. Case A.

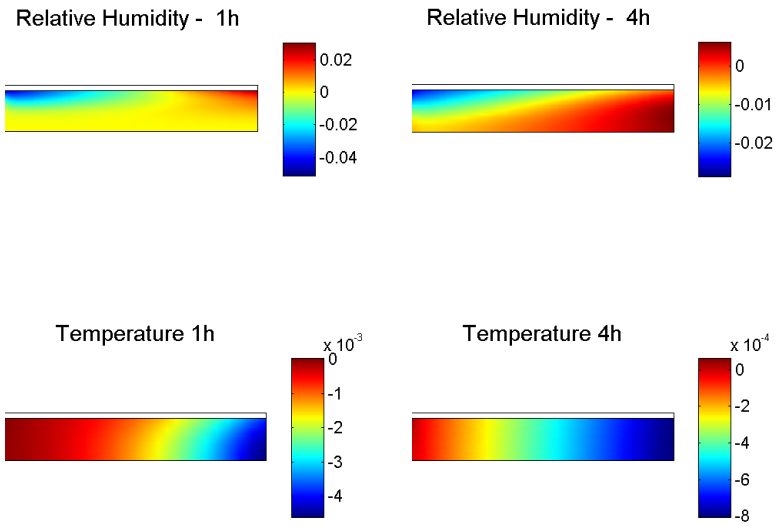

Figure 21: Relative differences between the conjugate and the line source approach, for temperature and relative humidity after 1 and 4 hours. Case A.

Case C In case C we have considered a gypsum square of 10 cm side, with a thin air channel, bending in the y direction (see figure 22). At the corner, the velocity field is no longer fully developed nor similar to the one that develops in a classic entry region. Therefore we can expect a discrepancy of the results from the two models at this position.

In this case, both the upper and the lower boundary of the channel interface with the porous material.

In table 7 are summarized temperature and relative humidity of the air at the channel inlet and initial conditions in the fluid and porous domains.

Table 7: Initial values (left) and air inlet values (right) of temperature and relative humidity for case C.

case	φ_0 [-]	T_0 [°C]	φ_{in} [-]	T_{in} [°C]
C	0.5	10	0.7	22

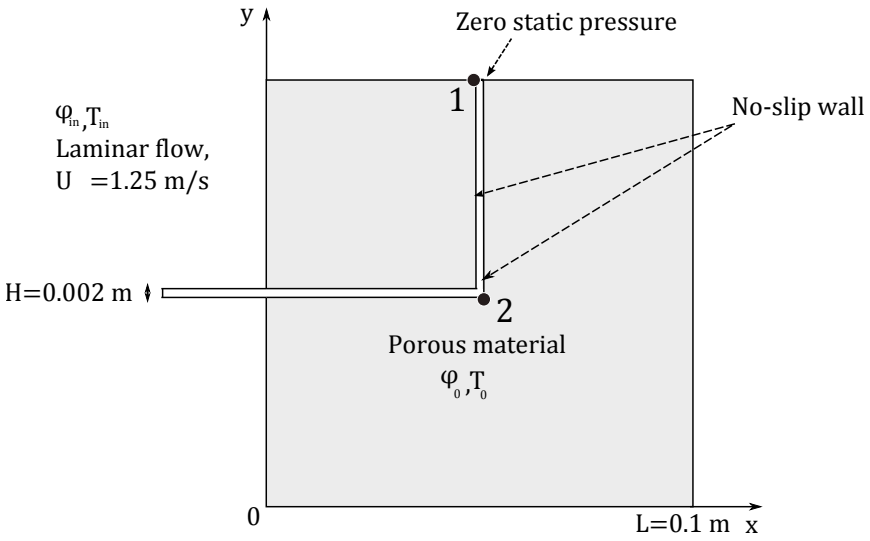

Figure 22: Geometry and boundary conditions for case C

In figure 23 the relative humidity and temperature distributions after one hour are shown. Figure 24 shows the relative difference between the two models at different times, calculated with equation 5.36. Consider that the relative difference of relative humidity after one hour can be as high as 15%, while at the same time, in cases A and B the absolute value of this difference was at maximum 7.1%. In figure 25 the temporal development of the relative error for relative humidity and temperature has been plotted out point 1 and 2 (see image 22).

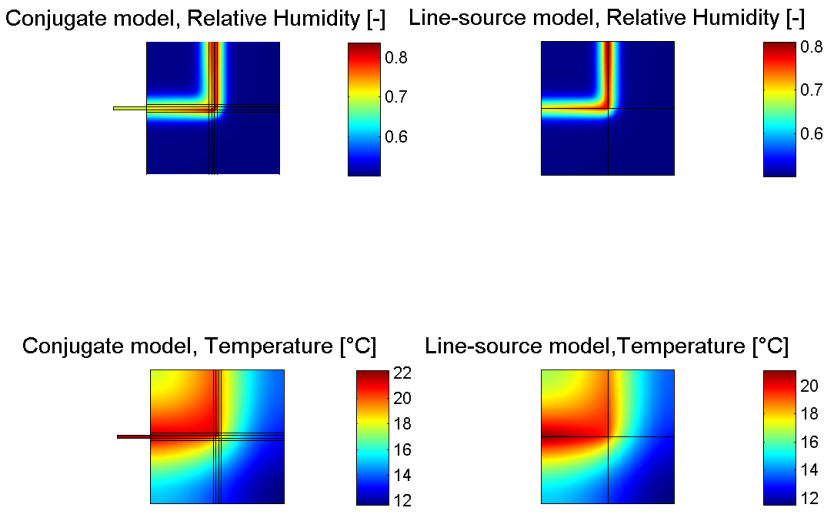

Figure 23: Relative humidity and temperature distributions for case C, after 1 h

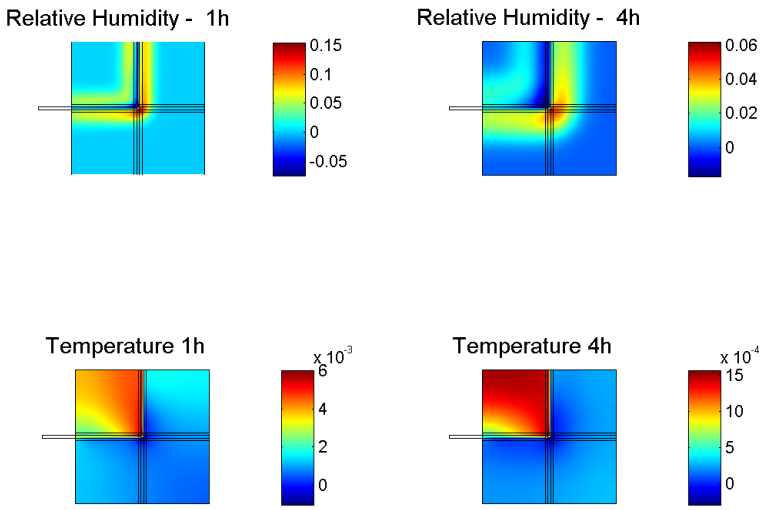

Figure 24: Relative differences between the conjugate and the line source approach, for temperature and relative humidity after 1 and 4 hours. Case C.

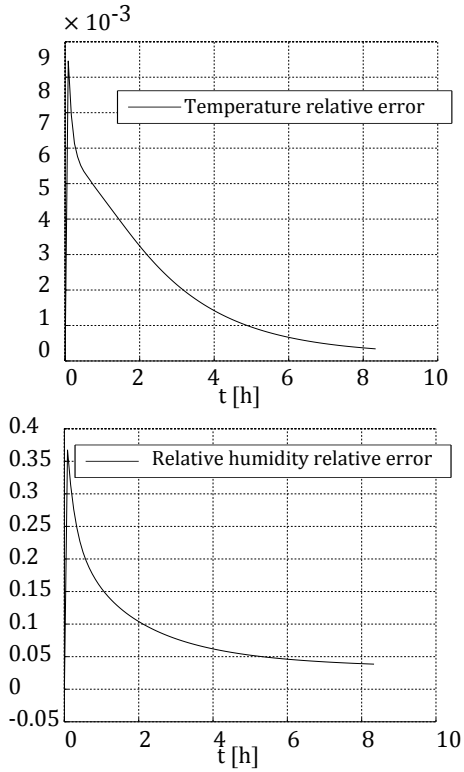

Figure 25: Temporal development of the relative error for T e φ in point 1 and 2 (see image 22)

6 Assessment of the equivalent thermal conductivity of an hollow brick

The model presented in this thesis can be applied in various building physics problems. A typical subject in building physics numerical simulations is to estimate the equivalent thermal conductivity (ETC), of a building material. This is particularly important for whole building heat analysis, in which the heat flux is calculated in simplified ways, since the main purpose is to analyze the dynamic thermal behavior of the building. An important case is the one of hollow bricks. Hollow bricks are widely used in constructions presenting goo thermal insulation and economical manufacturing. Inside the hollow bricks, a convective motion takes place due to the temperature differences on the side of the brick. This motion reduces the overall thermal insulation of the brick, leading to a decrease in the ETC.

As in [57] the ETC can be calculated as

$$ETC = \frac{qW}{|T_{in} - T_{ext}|} \tag{6.1}$$

where q is the total heat flux through the hollow brick, W , T_{in} and T_{ext} are the width of the hollow brick and the temperature on the internal and external surfaces. Even if the computation of hollow brick is a well studied problem, in most of the studies the influence of moisture is not considered [5, 4, 57]. For this reason, in the following simulations the influence of moisture over the ETC value will be investigated. Moisture can influence ETC esteem in two main ways:

1. Velocity field: since no total pressure gradients are considered, the air motion inside of the hollow brick is entirely generated by means of buoyancy forces. These buoyancy forces are generated by air density differences. Considering humid air as a mixture of ideal gases, these changes can be due to pressure, temperature and concentration variations. Since the pressure is considered to be constant inside the brick, only temperature and vapour concentration can cause buoyancy forces. In appendix 4.2, the influence of concentration and temperature on the fluid density is derived.

2. Enthalpy flow: the total heat transfer can be influenced by the enthalpy carried out by the outgoing vapour flux.

6.1 Preliminary study

For the following simulations, the same geometry and the same material properties proposed in [4] will be used. A first preliminary study, which does not take moisture transfer into account, is done in order to compare the temperature distribution presented in [4]. In figure 26, the geometry and the boundary conditions for this preliminary study are shown. Since the lack of information about the pressure inside the cavities makes it difficult to achieve convergence,

pressure at a point is arbitrary fixed to achieve faster computation [2]. In table 8, the geometric values and material properties of the brick are given.

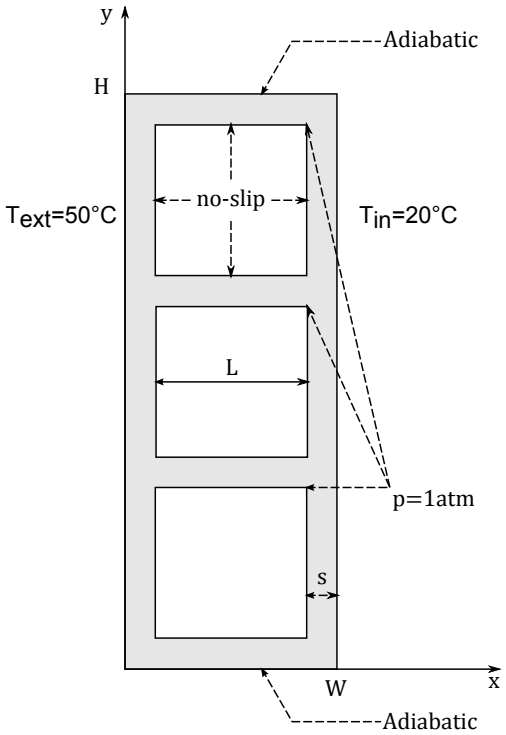

Figure 26: Geometry and boundary conditions for the first preliminary study

Table 8: Geometric parameters and material properties of the hollow brick.

L$[m]$	H$[m]$	s$[m]$	Density $\left[\frac{kg}{m^3}\right]$	c_m $\left[\frac{J}{kgK}\right]$	k_m $\left[\frac{W}{mK}\right]$
0.05	0.19	0.01	1800	840	1

Due to the small dimensions, the resulting Grashof number is in the order of 10^5, which is small enough for excluding the instauration of a turbulent flow regime inside the brick. Thus it is possible to consider the problem as two-dimensional, as done in [5],[63],[4] and [20]. Two different grid independence tests has been performed, the first considering heat transfer alone and the second with both heat and mass transfer equations. Three different grids has been used, with structured quadrilateral elements in the hollow parts of the brick,

and with free structured triangular mesh in the solid domain. In the second grid the elements have been halved and the free triangular mesh has been refined. The same procedure has been applied for the third grid. In both tests the L^2 norm for both temperature and humidity show a relative difference in the order of 10^{-4} between the second grid and the third grid results. Thus the second grid composed by 1220 quadrilateral elements and 2206 triangular elements has been used. The time-independent simulation is obtained with a relative tolerance of 10^{-4}, using a fully coupled solver, which solves the equations of momentum, heat and continuity simultaneously.

In figure 27 the isothermal lines for the first preliminary study are plotted, showing good agreement with the results of the reference study. The resulting value of the ETC is 0.91 $\left[\frac{W}{mK}\right]$.

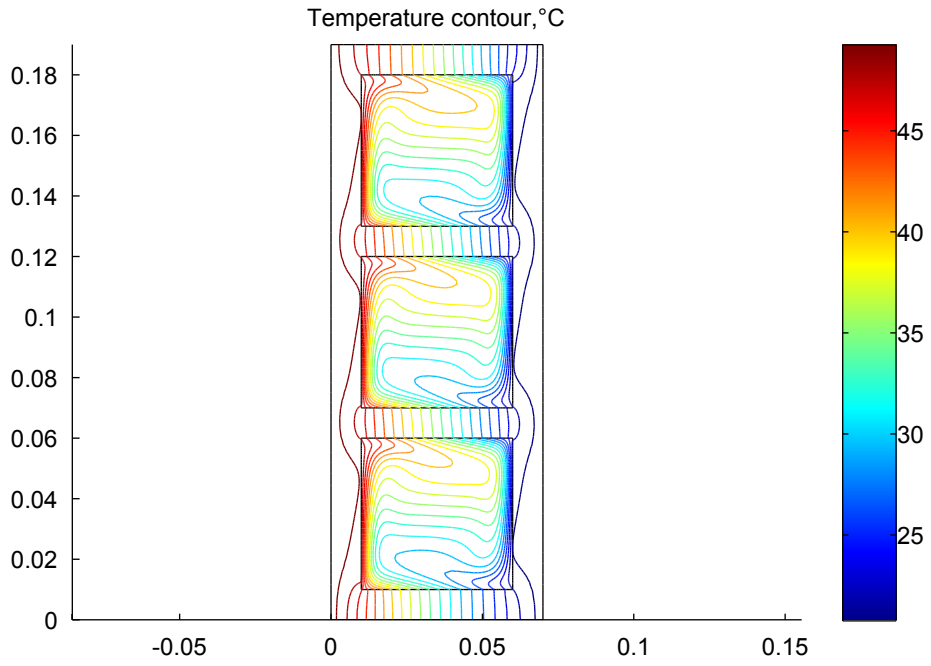

Figure 27: Isothermal lines for the preliminary study. The result show good agreement with the reference study [4]

6.2 Moisture influence

Using the conjugate model, the influence of moisture over total heat transfer is investigated. Dirichlet boundary conditions for relative humidity are imposed on the internal and external walls of the brick. The upper and lower parts of the brick are considered to be water-tight. Two cases are considered, with different temperature boundary conditions. In case A, a summer-like scenario is considered, with higher external temperature, while in case B a winter-like scenario is considered, with a lower external temperature. In both cases, the varying parameter are the internal and the external relative humidity boundary condition, which increases from 0.5 to 0.8 with a step of 0.1 . The temperature and relative humidity boundary conditions are shown in table 9.

Table 9: Temperature and relative humidity boundary conditions for case A and case B.

	$T_{ext}[°C]$	$T_{in}[°C]$	$\varphi_{ext}[-]$	$\varphi_{in}[-]$
CASE A	35	25	0.5,0.6,0.7,0.8	0.5,0.6,0.7,0.8
CASE B	10	20	0.5,0.6,0.7,0.8	0.5,0.6,0.7,0.8

For each case, 16 simulations are performed, one for each combinations of internal and external relative humidity boundary conditions. The time-independent solver uses a relative tolerance of 10^{-4}. Since the equations of momentum, heat and moisture transfer produce a strong nonlinear problem, solve them simultaneously is particularly challenging. Moreover, since the velocity field is caused by buoyancy forces, the problem represent a difficult convergence task for most nonlinear solvers. Therefore, the solution is achieved gradually increasing the value of gravity. When the value of gravity is setted to zero, the equations converge easily since momentum and temperature equations are uncoupled. Than the value of gravity is increased, and the solution of the previous step is used as initial guess for the next, until a value of 9.81 $\frac{m}{s^2}$ is reached. This is done activating a parametric sweep and choosing a scaling method of the independent variables based on their initial values. The independent variables are solved in a segregated way. The equations of heat and mass transfer are solved first, and than the velocity and pressure field are computed.

In each simulation, the heat flux is computed with three different models:

- Model 1: only heat transfer is taken into account. Buoyancy forces are only due to temperature differences.
- Model 2: heat and moisture transfer are computed, using the HAM model. Buoyancy forces are only due to temperature differences.
- Model 3: heat and moisture transfer are computed, using the HAM model. Buoyancy forces are due to temperature and moisture differences.

The parametric study can be easily performed interfacing Matlab with a COMSOL server [2]. A Matlab routine with a nested for loop is than needed for

varying the internal and external relative humidity boundary conditions. In this way the parametric simulation is automatically computed. In the same routine, the ETC values obtained with the three different models are compared. Since the wall temperatures in cases A and B are fixed, the only varying parameter in equation 6.1 is the heat flux, hence the relative ETC variation with respect to the third model, , is computed as

$$ETC_{rv,i} = \frac{ETC_3 - ETC_i}{ETC_i} = \frac{\overline{q_3} - \overline{q_i}}{\overline{q_i}} \tag{6.2}$$

where $\overline{q}$ is the average value of the heat flux, the subscript i refers to the model considered, either 1 or 2, and subscript 3 refers to the third model.

In figure 28 and 29 the relative ETC variations between the third and the first model are plotted, for cases A and B. For case A, the total increment of heat transfer due to considering moisture influence rather than ignoring it, can reach the maximum value of 19%. For case B the maximum increment is smaller, equal to 8.45%. In both the cases, the increment in ETC shows a similar behaviour. Firstly, the ETC relative difference increases for increasing differences of relative humidity boundary values. Secondly, it is more influenced by the relative humidity boundary value of the hotter side than it is by the relative humidity value on the colder side of the brick. These two effects can be explained considering that for the chosen range of boundary relative humidity (under 90%), capillary conductivity plays a minor role in the total humidity transfer. Most of the water transfer is caused by vapour diffusion inside the brick, that is due to concentration differences. The concentration of water vapour can be written as

$$x_v = \frac{\varphi p_s(T)}{p_g} \tag{6.3}$$

Considering p_g as constant, the concentration is influenced only by T and φ, and we can write

$$x_{v,c} - x_{v,h} = \frac{\varphi_h P_s(T_h) - \varphi_c P_s(T_c)}{p_g} \tag{6.4}$$

where the subscript h and c stands for the hot and cold side of the brick. Since the saturation pressure is an exponential function of T, the concentration difference is mostly influenced by the value assumed by φ_h.

In figure 30, the ETC_{rv} between the third and the second model are shown. The minor influence of φ_c on the ETC_{rv} is underlined, plotting the results in a two-dimensional graph. The maximum ETC relative increment for both cases A and B is of 0.1%, so the influence of vapour concentration on the velocity field can be neglected in this case.

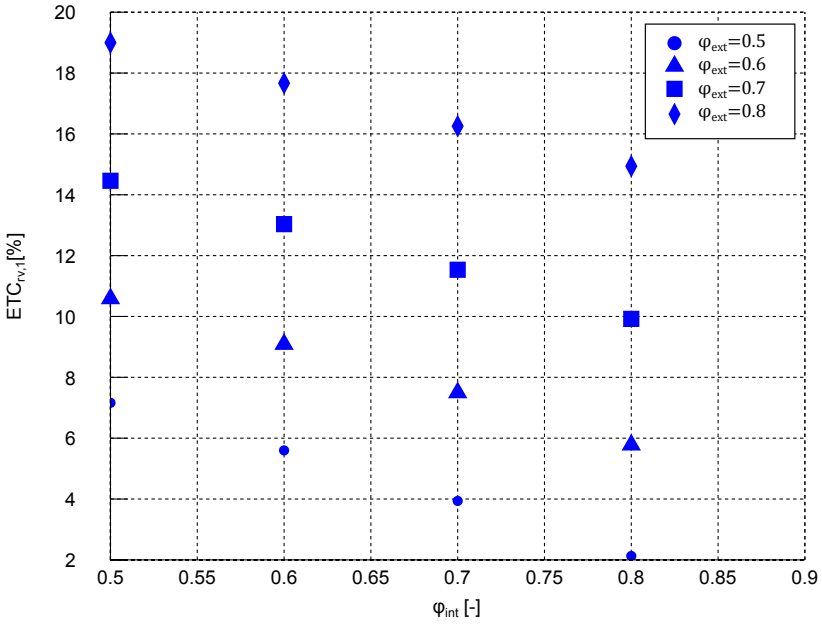

Figure 28: Relative increment of ETC due to the presence of humidity, for various combinations of relative humidity boundary conditions. Case A: $T_{ext} = 35°C$, $T_{in} = 25°C$.

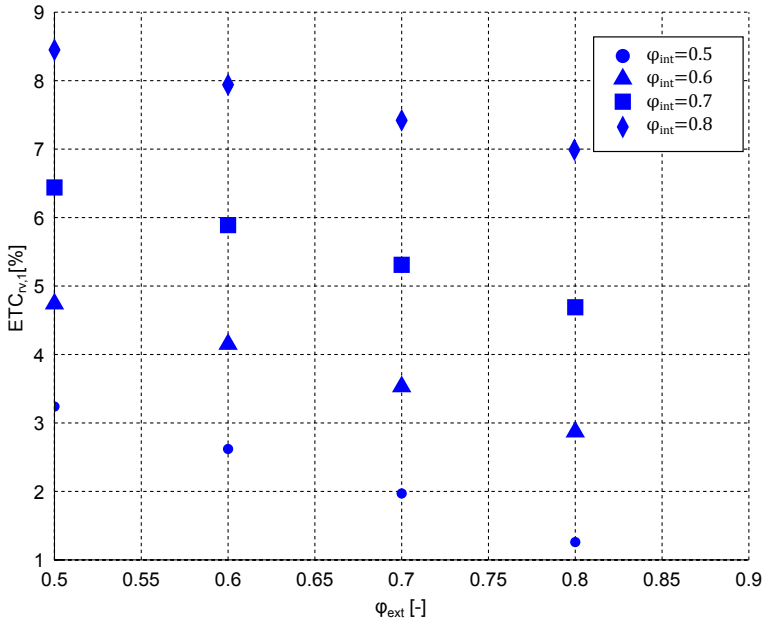

Figure 29: Relative increment of ETC due to the presence of humidity, for various combinations of relative humidity boundary conditions. Case B: $T_{ext} = 10°C$, $T_{in} = 20°C$.

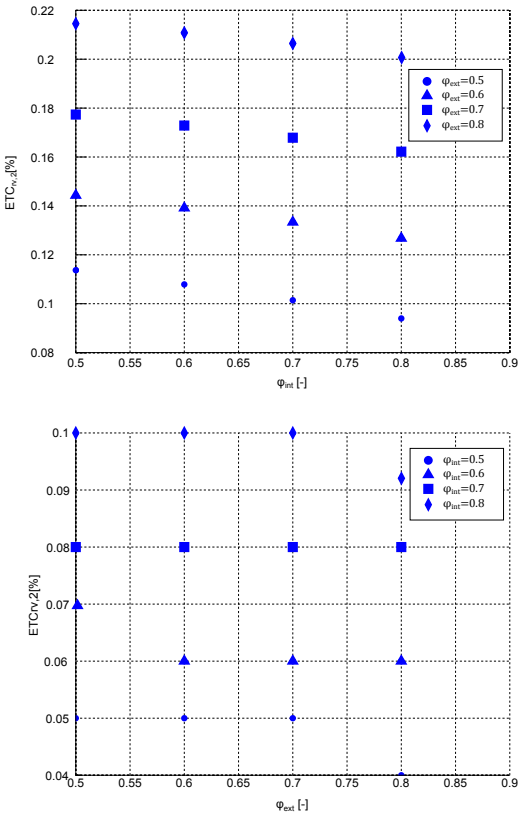

Figure 30: Relative increment of ETC caused by considering the influence of water concentration on gas density, rather than ignoring it. Up: case A $T_{ext} = 35°C$, $T_{in} = 25°C$, down: case B $T_{ext} = 10°C$, $T_{in} = 20°C$

7 Conclusions

7.1 Main results and conclusions

The main objective of this work was to implement in COMSOL an accurate model for heat and moisture analysis in porous building materials. For doing so, a conjugate model to describe the influence of air flow has been chosen, avoiding previous knowledge of CTCs. Validation of the model has been achieved by means of comparison with experimental data and with other numerical models.

The conjugate model has been used as a benchmark for the more simplified line-source model, which does not use CFD. Two cases have been studied in order to investigate the differences between the two models. In the first case a straight channel with laminar forced air flow has been simulated. After one hour, the relative differences in relative humidity between the conjugate and the line-source models assume a maximum value of 7%, while the maximum value of the relative difference of temperature is under 1% . In the second case, in which the channel vary his direction, the relative differences in relative humidity reach a maximum value of 15% after one hour. As expected, in this second case, the two models show higher discrepancies, since the constant CTCs used by the line source equations are obtained with fully-developed boundary layers.

In chapter 6, the conjugate model has been used to investigate the influence of moisture over the equivalent thermal conductivity of an hollow brick. Using a Matlab routine, a parametric study with changing relative humidity boundary conditions, comparing three different models, has been performed. The results show that the influence of moisture over buoyancy forces can be neglected, while the increase of heat transfer by means of enthalpy flow can be relevant. For the chosen range of temperature and relative humidity boundary conditions, the relative variation of the ETC can reach a value of 19%.

7.2 Further research

The comparison between the line-source and the conjugate model showed a significant discrepancy in the case of a bending channel. This discrepancy must be further investigated. In both simulations, the relative differences of the driving potentials between the two models decreases with time, as stationary conditions are being reached. In real hygrothermal simulations the steady state is never reached, since boundary conditions are typically time-dependent. A more complete study on the discrepancies between the models, can be achieved applying time-dependent boundary conditions, and computing the difference in total water content at the end of the simulation.

The high-level programming language of COMSOL allow to integrate additional physical phenomena and transport mechanisms that could be significant in problems other than the ones considered in this thesis. For example, heat transfer with the atmospheric air and with the ground due to radiation can be added using models for assessment of sky temperature, as in [27]. The direct and diffuse solar radiation can be considered as done in [58, 59] or [27]. In complex

geometry, surface-to surface radiation can be easily added, using a COMSOL pre-built module for the computation of view factors. Wind-driven rain effect can be considered by means of historical data as in [7, 42].

The results presented in this thesis concern laminar flow. Further work on the modeling of turbulent flow in air cavities will be performed, using a Low Reynolds number $k-\epsilon$ model, for the reason exposed in chapter 3.

In chapter 6, a laminar flow in natural convection has been studied, assuming stationary state. In real hygrothermal analysis the stationary state is never reached, since the boundary conditions constantly change. Further analysis could use time-dependent simulations to take into account the dynamic behaviour of the porous material.

8 Appendices

A Balance equations with T and φ as potentials

In order to simplify the balance equations, we assume the overall fluid as incompressible, that is:

$$\frac{\partial \rho_g}{\partial t} = 0 \tag{A.1}$$

which leads to $\nabla \cdot \mathbf{v} = 0$ and $\nabla \rho_g = 0$.
In addition we use ideal gas equation for the vapour.

A.1 Mass balance in porous media

$$\frac{\partial w}{\partial t} = -\nabla \cdot (J_v + J_l) \tag{A.2}$$

Using Fick's law for the diffusive vapour, and the law used by Künzel in [33] for diffusive liquid flux, we can write:

$$J_v = -\rho_g \frac{D_{av}}{\mu} \nabla \frac{\rho_v}{\rho_g} \tag{A.3}$$

$$J_l = K_l \frac{\partial p_c}{\partial \varphi} \nabla \varphi \tag{A.4}$$

Assuming incompressible flow, the first one can be written as:

$$J_v = -\frac{D_{av}}{\mu} \nabla \rho_v \tag{A.5}$$

We can now write ρ_v as a function of the potential φ, using the ideal gas equation and the definition of relative humidity.

$$\rho_v = \frac{p_v}{R_v T} = \frac{p_s \varphi}{R_v T} = F\varphi \tag{A.6}$$

This leads to:

$$J_v = -\frac{D_{av}}{\mu} (F \nabla \varphi + \varphi \nabla F) \tag{A.7}$$

Note that $F = \frac{Ps}{R_v T}$ is introduced in order to simplify notation. Note also that the saturation pressure is a function of temperature only. In this work we'll use the following formula

$$p_s = 610 exp \left(17.08085 \frac{\theta}{234.175 + \theta} \right) \tag{A.8}$$

with the temperature θ expressed in Celsius.

Applying the chain rule for the time derivative, substituting equations A.4 and A.7 in equation A.2, we can write:

$$\frac{\partial w}{\partial \varphi}\frac{\partial \varphi}{\partial t} = -\nabla \cdot (-D_{m\varphi p}\nabla\varphi - D_{mTp}\nabla T) \tag{A.9}$$

where w is the water content as a function of φ and with:

$$D_{m\varphi p} = \frac{D_{av}F}{\mu} - K_l\frac{\partial p_c}{\partial \varphi} \tag{A.10}$$

$$D_{mTp} = \varphi\frac{D_{av}}{\mu}\frac{\partial F}{\partial T} \tag{A.11}$$

A.1.1 Energy balance in porous media

The energy balance is described by equation A.12

$$\frac{\partial H_{pm}}{\partial t} = -\nabla \cdot (J_v h_v + J_l h_l + q^c) \tag{A.12}$$

where

$$h_v = c_{p,v}T + H_{ev} \tag{A.13}$$

$$h_l = c_{p,l}T \tag{A.14}$$

and

$$q^c = -k_{eff}\nabla T \tag{A.15}$$

Substituting equations A.4 and A.7 in equation A.12 , we obtain

$$\frac{\partial H_{pm}}{\partial t} = -\nabla \cdot (-D_{e\varphi p}\nabla\varphi - D_{eTp}\nabla T) \tag{A.16}$$

where

$$D_{e\varphi p} = \frac{D_{av}}{\mu}Fh_v - K_l\frac{\partial P_c}{\partial \varphi}c_{p,l}T \tag{A.17}$$

$$D_{eTp} = \frac{D_v}{\mu}\varphi\frac{\partial F}{\partial T}h_v + K \tag{A.18}$$

Applying the chain rule to the left hand term of A.16 we can write:

$$\frac{\partial H_{pm}}{\partial t} = \frac{\partial H_{pm}}{\partial T}\frac{\partial T}{\partial t} + \frac{\partial H_{pm}}{\partial \varphi}\frac{\partial \varphi}{\partial t} \tag{A.19}$$

Replacing the total enthalpy of the porous material with equation 4.16:

$$H_{pm} = \left(\rho_m c_{p,m} - wc_{p,a}\frac{\rho_a}{\rho_l} + wc_{p,l} + (w_{cp,s} - w)c_{p,v}\frac{\rho_v}{\rho_l}\right)T + (w_{cs} - w)H_{ev}\frac{\rho_v}{\rho_l} \tag{A.20}$$

where w_{cs} is the water content at capillary saturation. Note that the conservation equations for this model are not valid if the water content is above capillary saturation. Under such condition, moisture content is above critical moisture content for air transport, and the gaseous pressure cannot be assumed to be equal to the atmospheric pressure anymore.

Equation A.16 can be reformulated as:

$$d_T \frac{\partial T}{\partial t} + \nabla \cdot (-D_{e\varphi p} \nabla \varphi - D_{eTp} \nabla T) = -d_\varphi \frac{\partial \varphi}{\partial t} \tag{A.21}$$

where

$$d_T = \rho_m c_{p,m} + w \left(c_{p,l} - c_{p,a} \frac{\rho_a}{\rho_l} - c_{p,v} \frac{\rho_v}{\rho_l} \right) + w_{cs} c_{p,v} \frac{\rho_v}{\rho_l} + (w_{cs} - w)(c_{p,v} T + H_{ev}) \frac{\partial F}{\partial T} \frac{\varphi}{\rho_l} \tag{A.22}$$

$$d_\varphi = \frac{\partial w}{\partial \varphi} \left[c_{p,l} T - \frac{\rho_v}{\rho_l} (c_{p,v} T + Hev) - \frac{\rho_a}{\rho_l} c_{p,a} T \right] + \frac{(w_{cs} - w)}{\rho_l} (c_{p,v} T + H_{ev}) F \tag{A.23}$$

A.1.2 Vapour balance in fluid media

$$\frac{\partial \rho_v}{\partial t} = -\nabla \cdot (J_v) \tag{A.24}$$

where the convective vapour flux is defined as $J_v = \rho_v \mathbf{v_v}$. Considering the relative velocity of the vapour, due to diffusive effect, we can split the overall convective flux in the advective and diffusive flux, as:

$$J_v = \rho_v \mathbf{v_v} = \rho_v (\mathbf{v} + \mathbf{v_{r,v}}) = \rho_v \mathbf{v} - \rho D_{av} \nabla \frac{\rho_v}{\rho} \tag{A.25}$$

which can be simplified as before, under assumption of incompressible fluid flow as follows:

$$J_v^c = \rho_v \mathbf{v} - D_{av} \nabla \rho_v \tag{A.26}$$

The total velocity must be taken out from the divergence, in order to easily apply a fully developed flow condition. Using $\rho_v = F\varphi$
we obtain:

$$F \frac{\partial \varphi}{\partial t} + \nabla \cdot (-D_{m\varphi a} \nabla \varphi - D_{mTa} \nabla T) + \varphi \left(\frac{\partial F}{\partial t} + \mathbf{v} \frac{\partial F}{\partial T} \nabla T \right) + F \mathbf{v} \nabla \varphi = 0 \tag{A.27}$$

with

$$\begin{aligned} D_{mfa} &= D_{av} F \\ D_{mTa} &= D_{av} \varphi \frac{\partial F}{\partial T} \end{aligned} \tag{A.28}$$

A.1.3 Energy balance in fluid media

$$\frac{\partial H_g}{\partial t} = -\nabla \cdot (q^e + q^c) \tag{A.29}$$

where

$$q^e = J_v h_v + J_a h_a \tag{A.30}$$

We can replace the expression for the convective fluxes:

$$J_v = \mathbf{v}\rho_v - \rho_g D_{av} \nabla \frac{\rho_v}{\rho_g} \tag{A.31}$$

$$J_a = \mathbf{v}\rho_a - \rho_g D_{av} \nabla \frac{\rho_a}{\rho_g} \tag{A.32}$$

we obtain:

$$\frac{\partial H_g}{\partial t} = -\nabla \cdot \left[\left(\mathbf{v}\rho_v - \rho_g D_{av} \nabla \frac{\rho_v}{\rho_g} \right) h_v + \left(\mathbf{v}\rho_a - \rho_g D_{av} \nabla \frac{\rho_a}{\rho_g} \right) h_a - k_g \nabla T \right] \tag{A.33}$$

Reordering the right hand side , using the relation $\rho_g = \rho_v + \rho_a$, and considering a constant ρ_g:

$$\frac{\partial H_g}{\partial t} = -\nabla \cdot [\mathbf{v}(\rho_v(h_v - h_a) + \rho_g h_a) - D_{av}(\nabla \rho_v (h_v - h_a) + h_a \nabla \rho_g) - k_g \nabla T] \tag{A.34}$$

The air and vapour enthalpy are respectively defined as:

$$h_a = c_{p,a} T$$

and

$$h_v = c_{p,v} T + H_{ev}$$

Taking out the velocity term from the divergence, replacing $\rho_v = F\varphi$ and assuming incompressible flow, the right hand side can be rewritten as:

$$-\mathbf{v}(A_\varphi \nabla \varphi + A_T \nabla T) - \nabla \cdot (-D_{e\varphi a} \nabla \varphi - D_{eTa} \nabla T) \tag{A.35}$$

where

$$A_\varphi = (h_v - h_a) F \tag{A.36}$$

$$A_T = \varphi \frac{\partial F}{\partial T}(h_v - h_a) + \varphi F (c_{p,v} - c_{p,a}) + \rho c_{p,a} \tag{A.37}$$

$$D_{e\varphi a} = D_{av}(h_v - h_a) F$$

$$D_{eTa} = D_{av}(h_v - h_a) \varphi \frac{\partial F}{\partial T} + k_g \tag{A.38}$$

Using the mass fraction introduced in 2.11 , we can write the total gas enthalpy as

$$H_g = \rho_g h_g = \rho_g \left(m_v h_v + m_a h_a \right) \tag{A.39}$$

where

$$m_a = \frac{\rho_a}{\rho_g}$$

and

$$m_v = \frac{\rho_v}{\rho_g}$$

, the left hand term of equation A.34 can be rewritten as:

$$\frac{\partial H_g}{\partial t} = \frac{\partial(\rho_v h_v + \rho_a h_a)}{\partial t} \tag{A.40}$$

Using $\rho_g = \rho_a + \rho_v$, assuming incompressible flow and replacing $\rho_v = F\varphi$ we get:

$$\frac{\partial H_g}{\partial t} = \frac{\partial \varphi}{\partial t} F(h_v - h_a) + \frac{\partial T}{\partial t}\left[\varphi \frac{\partial F}{\partial T}(h_v - h_a) + F\varphi(c_{p,v} - c_{p,a}) + \rho_g c_{p,a}\right] \tag{A.41}$$

Using equation A.41 and A.42, equation A.34 becomes :

$$\begin{aligned} &\frac{\partial \varphi}{\partial t} F(h_v - h_a) + \frac{\partial T}{\partial t}\left[\varphi \frac{\partial F}{\partial T}(h_v - h_a) + F\varphi(c_{p,v} - c_{p,a}) + \rho_g c_{p,a}\right] = \\ &\qquad -\mathbf{v}(A_\varphi \nabla\varphi + A_T \nabla T) - \nabla \cdot (-D_{e\varphi a}\nabla\varphi - D_{eTa}\nabla T) \end{aligned} \tag{A.42}$$

B Additional considerations on natural convection in presence of moisture

Additional considerations can be done using the nondimensional form of the momentum equation. To do this, we can define a nondimensional velocity

$$\mathbf{V} = \frac{\mathbf{v_g}}{U} \tag{B.1}$$

where U is a characteristic velocity, and a nondimensional spatial vector

$$\mathbf{X} = \frac{\mathbf{x}}{L} \tag{B.2}$$

where L is a characteristic length scale. Using equation B.1 and B.2 along with 4.28 the nondimensionalization process leads to

$$\frac{1}{U}\frac{\partial(\mathbf{V})}{\partial t} + \nabla \cdot (\mathbf{V} \otimes \mathbf{V}) = \nabla \cdot \left(-\frac{p_d \mathbf{I}}{\rho_g U^2} + \frac{\mu}{\rho_g L U}\nabla \mathbf{V}\right) + \frac{\mathbf{g}\rho_g L}{\rho_g U^2} \tag{B.3}$$

where the last term can be rewritten as

$$\frac{Gr}{Re^2} = Ri$$

where Gr is the Grashof number, Re is the Reynolds number and Ri is the Richardson number, which is the ratio of buoyancy forces over inertial forces. When $Ri \ll 1$, the buoyancy effect can be neglected, and the problem can be considered to be of pure convection. Even if density differences are usually taken into account through a temperature difference, the final nondimensionalized equations are exactly the same. This means that transition from laminar to turbulent flow occurs for the same critical Grashof number. In the case of a vertical plate the critical Grashof number is between 10^8 and 10^9 according to [41].

C Space and time numerical discretization

C.1 Numerical diffusionsection

The system of coupled partial differential equations (A.9 and A.21 inside the porous domains and 4.23 ,4.28,A.27 and A.42 inside the fluid domains) has to be solved using a numerical schema which introduces approximation errors.

These approximation errors in the computed solutions are also known as numerical diffusion or truncation errors [36].

For a simple example, we can consider the first order wave equation:

$$\frac{\partial u}{\partial t} + c\frac{\partial u}{\partial x} = 0 \tag{C.1}$$

Where c is the velocity.

For the sake of notation simplicity we can use subscripts to indicate partial derivatives:

$$u_t + cu_x = 0 \tag{C.2}$$

We can now choose to use the explicit Euler method for time differentiation, which leads to:

$$u^1 - u^0 + c\Delta t u_x^1 = 0 \tag{C.3}$$

with the superscript indicating the time step in which the solution is calculated.

We have not done any assumption on the spatial discretization so far, since the effect of time and spatial discretization on the solution can be

discussed separately.

Equation C.3 is used by the numerical solver to find a solution. It can be shown that this discretized equation introduces an error that depends on the

time step. Let's consider the second order Taylor series with respect to time step:

$$u^1 = u^0 + u_t\Delta t + u_{tt}^0\frac{(\Delta t)^2}{2} \tag{C.4}$$

and the first order Taylor series for u_x:

$$u_x^1 = u_x^0 + u_{xt}^0\Delta t \tag{C.5}$$

Substituting in equation C.3, we have:

$$u_t^0 + u_{tt}^0\frac{\Delta t}{2} + cu_x^0 + c\Delta t u_{xt}^0 = 0 \tag{C.6}$$

We can now obtain u_{xt}^0 and u_{tt}^0 as function of u_{xx}^0. Differentiating the analytic equation once in respect to x and once in respect to t, we can find:

$$u_{tt} = -cu_{xt} \tag{C.7}$$

$$u_{tx} = -cu_{xx} \tag{C.8}$$

$$u_{tt} = c^2 u_{xx} \tag{C.9}$$

Substituting in the previous equation, we have:

$$u_t^0 + cu_x^0 = c^2 \frac{\Delta t}{2} u_{xx}^0 \tag{C.10}$$

This shown that discretizing with a explicit Euler method introduces a diffusion-like term in the discretized equation.

$$c^2 \frac{\Delta t}{2} \tag{C.11}$$

is called numerical diffusivity. It's easy to see that this term will reduce linearly with the time step, so equation C.10 reduces to equation C.2 for very small time steps.

A similar procedure can be used for the spatial discretization, which introduces

$$\frac{ch}{2} u_{xx}^0 \tag{C.12}$$

in the discretized equation, where h is the discretization length. If a finite volume method is used, additional approximations are necessary in order to obtain the values of the variables and fluxes at cell boundaries. This additional passage is not necessary using a finite element method, in which only the values at the nodes are used to compute the solution.

It is well known that a modification of the discretized equation is possible in order to achieve a smaller truncation error [36] (pg.117). However this can not be easily done for non linear equations, or when a non fixed time-step algorithm is used, as in the case of COMSOL.

C.2 Stabilization techniques

The energy and mass conservation equations are written in the form of a generic scalar-convection transport equation

$$\frac{\partial u}{\partial t} + \mathbf{v} \cdot \nabla u = \nabla \cdot (c \nabla u) + F$$

The Péclet number, defined as

$$Pe = \frac{\mathbf{v} h}{2c} \tag{C.13}$$

where h is the mesh size, is a measure of the relative importance of the convective effects compared to the diffusive effects; a large Péclet number indicates that the convective effects dominate over the diffusive effects [39] .

As long as diffusion is present there is always a theorical mesh resolution for which the discretization is stable. This means that oscillations due to steep

gradient or space dependent initial conditions that the mesh does not resolve can be removed refining the mesh.

In practice this method could require a very dense mesh, and for this reason it is common practice to use stabilization methods. COMSOL uses various stabilization methods by default in many pre-built physics interfaces, as well as the laminar and turbulent flow interfaces, but the general form, weak form and coefficient form interfaces lack a pre-built stabilization.

If the equations show an unstable behaviour, is therefore necessary to include such a technique by adding a weak form contribution.

In the simulations performed in this thesis, even if the Péclet number largely exceeded unity, the transport equations show a stable behaviour. The implementation of a subgrid scale method as described in [34, 12], showed little influence over the results, thus it was omitted in this thesis.

C.3 Numerical influence of the material properties

Is widely recognized that the numerical quality of the solution is influenced by the material properties since the non linearity of the problem. For example, uncertainties in material property are identified to be the main cause in the discrepancy between simulations and experimental data in a study carried out for IEA/ECBCS Annex 41(International Energy Agency/Energy Conservation in Building and Community Systems) [24],[25]. Is indeed possible to show this influence with a sensitivity study.

Since the equations uses material properties that are moisture-dependent, it is important to ensure the limitations of those quantities, in case of little oscillations of the relative humidity over the unity value or below zero.

This is particularly evident in the case of the water storage function. The water storage function is a property of the porous material and is obtain by means of experiments. Is therefore used as an interpolated function of discrete values. However, is necessary to extrapolate this function, since if the value of ϕ slightly exceeds unity during the computation, convergence could not be reached. This is done keeping the same derivative with respect to relative humidity in $\varphi = 1$.

Another case in which is important to have a control over the value of relative humidity is related to capillary pressure. The capillary pressure is expressed as a function of φ through the Kelvin's formula:

$$p_c = -\rho_w R_v T ln(\varphi) \tag{C.14}$$

Since for negative values of the variable φ equation C.14 loses physical meaning, it is important to ensure the non negativity of φ.

For this reason, an additional variable C is introduced, defined as follows:

$$C(\varphi) = \begin{cases} eps, & if \varphi < eps \\ \varphi, & if \varphi > eps \end{cases} \tag{C.15}$$

where *eps* is the smallest number that can be used in calculations by the computer. This is a pre-defined constant in COMSOL. Instead of equation C.14, the following equation is employed in the model:

$$p_c = -\rho_w R_v T ln(C) \tag{C.16}$$

References

[1] http://www.bauklimatik-dresden.de/delphin/index.php 1.

[2] © COMSOL AB. Comsol 4.3a documentation. 1998-2012.

[3] International Energy Agency, Energy Conservation In, and Community Systems. International Energy Agency: Guidelines & Practice. 2, 1990.

[4] Majed M. Al-Hazmy. Analysis of coupled natural convection conduction effects on the heat transport through hollow building blocks. *Energy and Buildings*, 38(5):515–521, May 2006.

[5] K Arendt, M Krzaczek, and J Florczuk. International Journal of Thermal Sciences Numerical analysis by FEM and analytical study of the dynamic thermal behavior of hollow bricks with different cavity concentration. *International Journal of Thermal Sciences*, 50(8):1543–1553, 2011.

[6] R Byron Bird, Warren E Stewart, and Edwin N Lightfoot. *Transport phenomena*. Wiley. com, 2007.

[7] Bert Blocken, Staf Roels, and Jan Carmeliet. A combined CFD-HAM approach for wind-driven rain on building facades. 31(0):585–607, 2007.

[8] Martin J Blunt. Flow in porous media pore-network models and multiphase flow. *Current opinion in colloid & interface science*, 6(3):197–207, 2001.

[9] Reint Boer, Instytut Podstawowych Problemów Techniki, and Polska Akademia Nauk. *Porous media: a survey of different approaches*. Universität-GH-Essen, Fachbereich 10–Bauwesen, 1991.

[10] A Bradji and E Holzbecher. On the Convergence Order of COMSOL Solutions. (3):2–7, 1999.

[11] Celia. A General Mass-Conservative Numerical Solution for the UNsaturated Flow Equation, 1990.

[12] Ramon Codina. Comparison of Some Finite Element Methods for Solving the Diffusion-Convection-Reaction Equation. 156:185–210, 1998.

[13] Thijs Defraeye. *Convective heat and mass transfer at exterior building surfaces*. Number January 2011. 2011.

[14] Thijs Defraeye, Bert Blocken, Dominique Derome, Bart Nicolai, and Jan Carmeliet. Convective heat and mass transfer modelling at air porous material interfaces: Overview of existing methods and relevance. *Chemical Engineering Science*, 74(1):49–58, May 2012.

[15] Willard Gardner and John A Widtsoe. The movement of soil moisture. *Soil Science*, 11(3):215–232, 1921.

[16] H. Gertis, K. und Erhorn. *Increased insulation in buildings - a way to avoid the coming change in climate?* Bauphysik 13 H.5, S. 132-137, 1991.

[17] Matthias K Gobbert. A Technique for the Quantitative Assessment of the Solution Quality on Particular Finite Elements in COMSOL Multiphysics.

[18] Matthias K Gobbert and Shiming Yang. Numerical Demonstration of Finite Element Convergence for Lagrange Elements in COMSOL Multiphysics. 2008.

[19] J. Grunewald. *Diffusiver und konvektiver Stoff- und Energietransport in kapillarporösen Baustoffen.* Dresdner bauklimatische Hefte. TU Dresden, 1997.

[20] Gerson Henrique and Nathan Mendes. Heat, air and moisture transfer through hollow porous blocks. *International Journal of Heat and Mass Transfer*, 52(9-10):2390–2398, 2009.

[21] H.S.L.C. Hens, Air IEA Energy Conservation in Buildings & Community Systems Programme. Annex 24-Heat, Moisture Transfer through New, Retrofitted Insulated Envelope Parts, and Laboratorium Bouwfysica. Departement Burgerlijke Bouwkunde. *Heat, Air and Moisture Transfer in Insulated Envelope Parts: Task 1, Modelling, Final Report.* Laboratorium Bouwfysica, Departement Burgerlijke Bouwkunde, 1996.

[22] OA Hougen, HJ McCauley, and WR Marshall Jr. Limitations of diffusion equations in drying. *Trans. AIChE*, 36:183–210, 1940.

[23] Frank P Incropera, Adrienne S Lavine, and David P DeWitt. *Fundamentals of heat and mass transfer.* John Wiley & Sons Incorporated, 2011.

[24] Chris James, Carey J. Simonson, Prabal Talukdar, and Staf Roels. Numerical and experimental data set for benchmarking hygroscopic buffering models. *International Journal of Heat and Mass Transfer*, 53(19-20):3638–3654, September 2010.

[25] Christopher Michael James. Heat and Moisture Transfer in a Bed of Gypsum Boards. (April), 2009.

[26] M Bianchi Janetti, F Ochs, and W Feist. Numerical Quality of a Model for Coupled Heat and Moisture Transport in COMSOL Multiphysics. 2012.

[27] Hans Janssen, Bert Blocken, and Jan Carmeliet. Conservative modelling of the moisture and heat transfer in building components under atmospheric excitation. *International Journal of Heat and Mass Transfer*, 50(5-6):1128–1140, March 2007.

[28] A Kalagasidis, P Weitsmann, T Nielson, R Peuhkuri, C Hagentoft, and C Rode. The international building physics toolbox in simulink. 39:2013, 2007.

[29] Ahmet Kaya. Numerical modeling of heat and mass transfer during forced convection drying of rectangular moist objects. *International Journal of Heat and Mass Transfer*, 49(17-18):3094–3103, August 2006.

[30] O Krischer and H Rohnalter. Heat and mass transfer in drying. *VDI-Forschungsh*, 11, 1940.

[31] Martin Krus. *Moisture Transport and Storage Coefficients of Porous Mineral Building Materials.* PhD thesis, Fraunhofer-Institurt für bauphysik, 1996.

[32] H. Kunzel. Verfahren zur ein- und zweidimesionalen Berechnung des dekoppelten Warme und Feuchtetransports in Bauteilen mit einfachen Kennwerten. page 1994, 1994.

[33] Hartwig M Künzel. *Simultaneous Heat and Moisture Transport in Building Components One- and two-dimensional calculation using simple parameters* ., volume 1995. IRB-Verl., 1995.

[34] Dmitri Kuzmin. A Guide to Numerical Methods for Transport Equations. 2010.

[35] Jerzy Kwiatkowski, Kamil Feret, Monika Woloszyn, and Jean-jacques Roux. Predicting indoor relative humidity using building energy simulation tools. 33, 2003.

[36] Randall J Leveque. *Numerical Methods for Conservation Laws.* 1992.

[37] WK Lewis. The rate of drying of solid materials. *Industrial & Engineering Chemistry*, 13(5):427;432, 1921.

[38] Aleksej Luikov. *Heat and mass transfer in capillary-porous bodies.* Pergamon Press, 1966.

[39] H K Versteeg Malalasekera and W. *An Introduction to Computational Fluid Dynamics*, volume M. 2007.

[40] E. E. Miller and R. D. Miller. Physical Theory for Capillary Flow Phenomena. *Journal of Applied Physics*, 1956.

[41] Alina A Minea. *Advances in industrial heat transfer.* CRC Press, 2012.

[42] Martin Morelli. MAJOR CHANGES WERE MADE TO THE FINAL VERSION OF THE PAPER METHOD FOR INVESTIGATION OF INTERIOR POST-INSULATED. pages 1–33, 2012.

[43] Yechezkel Mualem. A Conceptual Model of Hysteresis. *Water Resources Research*, 10, 1974.

[44] S Murakami. Comparison of various turbulence models applied to a bluff body. *Journal of Wind Engineering and Industrial Aerodynamics*, 46:21–36, 1993.

[45] A. Nicolai. *Modeling and Numerical Simulation of Salt Transport and Phase Transitions in Unsaturated Porous Building Materials*. Syracuse University, 2008.

[46] C.J. Simonson O.F. Osanyintola, P. Talukdar. E ect of initial conditions , boundary conditions and thickness on the moisture bu ering capacity of spruce plywood. 38(10), 2006.

[47] Olalekan F. Osanyintola and Carey J. Simonson. Moisture buffering capacity of hygroscopic building materials: Experimental facilities and energy impact. *Energy and Buildings*, 38(10):1270–1282, October 2006.

[48] Chen Peishi and David CT Pei. A mathematical model of drying processes. *International Journal of Heat and Mass Transfer*, 32(2):297–310, 1989.

[49] Alf Perschk and Uwe Meinhold. Ein Modell zur hygrisch-thermischen Gebäudesimulation mit Hilfe der Kopplung von Zonen- und Feldmodell. *Bauphysik*, 29(1):55–62, February 2007.

[50] JR Philip and DA De Vries. Moisture movement in porous materials under temperature gradients. *Transactions, American Geophysical Union*, 38:222;232, 1957.

[51] Lorenzo Adolph Richards. Capillary conduction of liquids through porous mediums.

[52] TK Sherwood. The drying of solids i. *Industrial and Engineering Chemistry*, 21(1):12–16, 1929.

[53] TK Sherwood. The drying of solids ii. *Industrial and Engineering Chemistry*, 21(10):976–980, 1929.

[54] Delphin Software. http://www.bauklimatik-dresden.de/delphin/. 2011.

[55] Wufi Software. http://www.wufi.de/. 2011.

[56] H.-J. Steeman, M. Van Belleghem, a. Janssens, and M. De Paepe. Coupled simulation of heat and moisture transport in air and porous materials for the assessment of moisture related damage. *Building and Environment*, 44(10):2176–2184, October 2009.

[57] Jiapeng Sun and Liang Fang. Numerical simulation of concrete hollow bricks by the finite volume method. *International Journal of Heat and Mass Transfer*, 52(23-24):5598–5607, November 2009.

[58] F Tariku and M K Kumaran. Hygrothermal modeling of aerated concrete wall and comparison with field experiment. pages 321–328, 2006.

[59] Fitsum Tariku. *Whole building heat and moisture analysis*. Number April. 2008.

[60] David W Trott and Matthias K Gobbert. Finite Element Convergence for Time-Dependent PDEs with a Point Source in COMSOL 4 . 2. 2:1–6.

[61] David W Trott and Matthias K Gobbert. Conducting Finite Element Convergence Studies using COMSOL 4.0. 2, 2010.

[62] Adrianus Wilhelmus Maria van Schijndel. *Integrated Heat Air and Moisture Modeling and Simulation*. 2007.

[63] C. Vasile. Study of convective phenomena inside cavities coupled with heat and mass transfers through porous media- application to vertical hollow bricks-a first approach. *Energy and Buil*, 28:229–235, 1998.

[64] Stephen Whitaker. Simultaneous Heat, Mass, and Momentum Transfer in Porous Media: A Theory of Drying. 13:119–203, 1977.